

Electronic Supporting Information

Integrated Multistep Photochemical and Thermal Continuous Flow Reactions; Production of Bicyclic Lactones with Kilogram Productivity.

Rowena A. Howie,^a Luke D. Elliott,^b Surajit Kayal,^a Xue-Zhong Sun,^a Magnus W. D. Hanson-Heine,^a Jonathan Hunter,^a Charlotte A. Clark,^a Ashley Love,^a Christopher Wiseall,^a Darren S. Lee,^a Martyn Poliakoff,^a Kevin I. Booker Milburn^b and Michael W. George^{*a,c}

^aSchool of Chemistry, University of Nottingham, University Park, Nottingham, NG7 2RD, UK.

^bSchool of Chemistry, University of Bristol, Cantock's Close, Bristol, BS8 1TS, UK.

^cDepartment of Chemical and Environmental Engineering, University of Nottingham Ningbo China, 199 Taikang East Road, Ningbo, 315100, China.

*Email: mike.george@nottingham.ac.uk

Table of Contents

1. General Experimental	S3
2. Initial Studies on Photochemical and Thermal Steps.....	S4
3.1. Optimization of the [2+2] Photochemistry of 1a and 2a.	S4
2.1.1 Sensitizer Screen in Batch	S4
2.1.2. Solvent Screen with ITX in Batch.....	S5
2.1.3. Screening Concentration and Lamp Power.....	S5
2.1.4. Transfer to Large Scale Continuous Flow Reactor with a 3 kW Lamp – Predicting the Flow Rate From Batch Results	S6
2.2. Homogenous Lactone Hydrolysis Investigation in Batch	S7
2.3. Biphasic Lactone Hydrolysis / Aqueous Ring Opening Sequence	S8
2.4. Initial Linking of Flow Photochemical and Batch Thermal Reactions	S9
2.4.1. 1 Mole Scale Photo/Thermal Reaction Sequence.....	S9
2.4.2. 5 Mole Scale Photo/Thermal Reaction Sequence.....	S9
3. High Temperature Water (HTW) Reactor Set-ups	S11
3.1. Reactor Description and Details.....	S11
3.1.1. Large Scale Thermal Flow Reactor	S11
3.1.2. Small Scale Thermal Flow Reactor	S12
3.1.3. Standard Operating Procedure for Thermal Flow Reactors	S13
3.1.4. Batch Thermal Reactions	S14
3.2. Photochemical Flow Reactor linked with HTW Reactor	S14
3.2.1. Photochemical Set-up	S14

3.2.2. Linking of the Photochemical Flow reactor with the HTW Reactor.....	S15
3.2.3. Batch Photochemical Reactions.....	S15
4. Optimisation of Thermal Reaction in High Temperature Water	S16
4.1. Batch Ring Expansion/Lactonization of 6a in High Temperature Water/Acetonitrile Mixtures	S16
4.2. Continuous Flow Ring Expansion/Lactonization of 6a in High Temperature Water/Acetonitrile Mixtures	S17
4.3. Continuous-Flow Combined Hydrolysis and Ring Opening	S18
5. Batch Photochemistry of Additional Substrates	S19
6. Optimisation of Small Scale Thermal Reactor for the Ring expansion of 5b and 5c.....	S20
7. Characterization Data	S22
8. NMR Spectra	S27
9. Time Resolved Infrared Spectroscopy (TRIR).....	S34
9.1. Description of Time Resolved Infrared Spectroscopy (TRIR) setup	S34
9.2. Time Resolved Infrared Data	S35
9.3. Characterization of the transient species	S37
9.4. Kinetic rate constants for the sensitized reaction	S37
10. Raman Monitoring	S40
10.1. Photochemical step.....	S40
10.2. Thermal steps.....	S41
11. gProms Modelling	S43
11.1. Model Description.....	S43
12. Density Functional Theory Calculations.....	S44
13. References	S48

1. General Experimental

Reagents, solvents and gases were purchased from commercial suppliers and used without further purification, unless otherwise described.

Proton nuclear magnetic resonance (^1H NMR) spectra and proton-decoupled carbon nuclear magnetic resonance (^{13}C NMR) spectra were recorded at 25 °C (unless stated otherwise) using Bruker AV400 (400 MHz) and AV(III)400hd (400 MHz) spectrometers. Chemical shifts for proton are reported in parts per million downfield from tetramethylsilane and are referenced to residual protium in the NMR solvent according to values reported in the literature. Chemical shifts for carbon are reported in parts per million downfield from tetramethylsilane and are referenced to the carbon resonances of the solvent. The solvent peak was referenced to 7.26 ppm for ^1H and 77.16 ppm for ^{13}C in CDCl_3 .

Data are represented as follows: chemical shift, integration, multiplicity (s = singlet, d = doublet, t = triplet, q = quartet, m = multiplet), coupling constants (J) is in Hertz (Hz). NMR spectra were processed with MestReNova Software (v 12.0.4-22023).

Yields and conversions for flow experiments were determined by ^1H NMR using biphenyl as an internal standard.

2. Initial Studies on Photochemical and Thermal Steps

3.1. Optimization of the [2+2] Photochemistry of 1a and 2a.

2.1.1 Sensitizer Screen in Batch

A screen of commercially available sensitizers identified isopropylthioxanthone (ITX) as the optimal sensitizer for the [2+2] cycloaddition of THPA with propargyl alcohol (Figure S1). As previously reported for kilogram scale synthesis examples,^[1] ITX is preferred over the parent thioxanthone for synthesis and process applications due to its increased solubility in organic solvents. Compared to the unsensitized reaction, productivity was increased by 10× using ITX, representing a large increase in energy efficiency for the reaction. Under these conditions, benzophenone is only marginally less productive than ITX but the greater extinction coefficient of ITX over BP allows it to be used at lower concentrations with minimal loss of UV transmission and hence productivity.

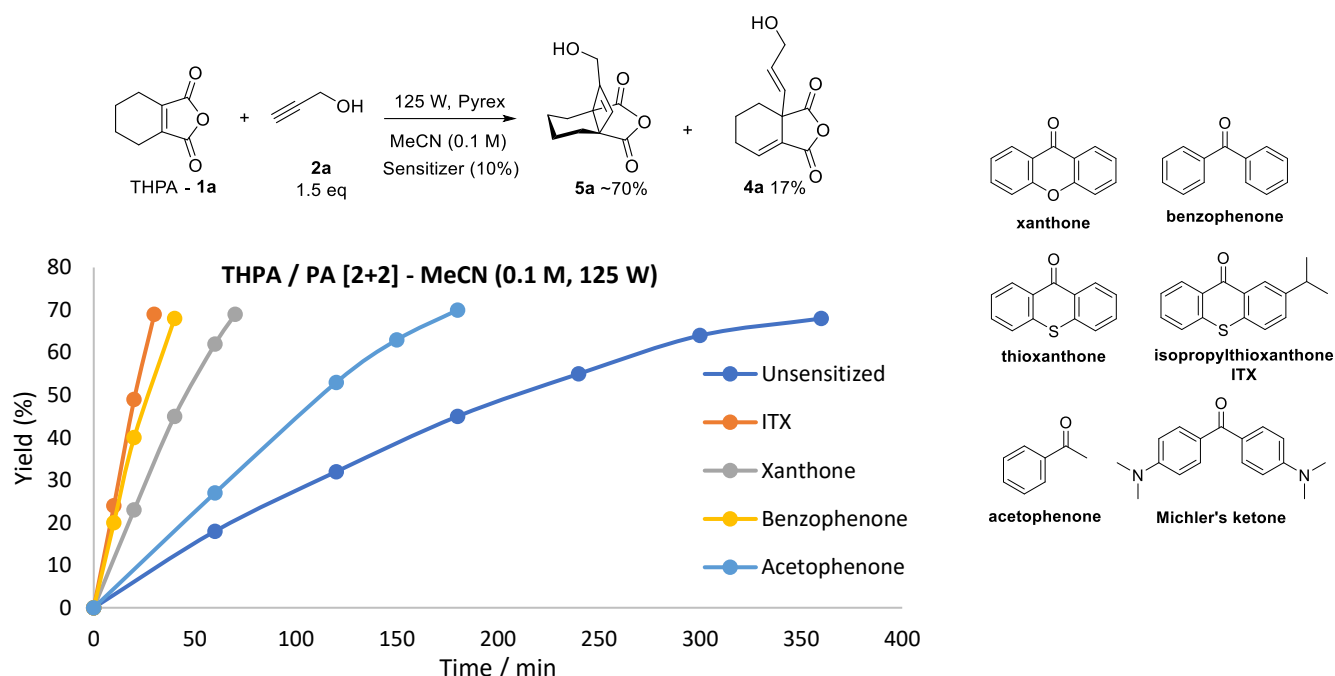


Figure S1: Reaction profiles for irradiation of THPA and propargyl alcohol in MeCN (0.1 M) for sensitized (10%) and unsensitized reactions in a 150 ml Pyrex immersion well batch reactor with 125 W Hg lamp

Table S1: Initial productivities for [2+2] of THPA with propargyl alcohol for the sensitizer screen in MeCN (0.1 M, 10% sensitizer, 150 ml Pyrex reactor, 125 W Hg lamp)

Sensitizer	E _r (kJ/mol)	Initial productivity (mmol/h)
None	n.a.	2.7
Acetophenone	310 (n)	4
Xanthone	310 (n)	10
Benzophenone	287 (n)	18
Thioxanthone	265 (n)	22
Michler's	255 (p)	No reaction

2.1.2. Solvent Screen with ITX in Batch

Having identified isopropylthioxanthone as the optimal sensitizer in acetonitrile, a solvent screen was carried out at the increased concentration of 0.5 M and ITX loading of 1% (Figure S2). EtOAc was identified as the optimal solvent for the reaction giving a superior productivity to the standard MeCN solvent. Its lower cost, toxicity and environmental impact are also attractive features which fit well within the aims of the current work.

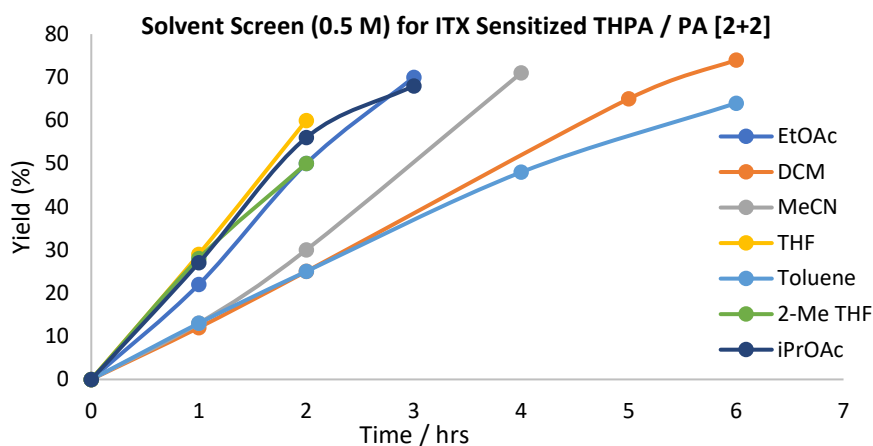


Figure S2: THPA / PA solvent screen (0.5 M, 150ml 1% ITX, 125 W Hg)

2.1.3. Screening Concentration and Lamp Power

The optimized solvent (EtOAc) and sensitizer (ITX) conditions were used to screen batch reactions with an increased lamp power of 400 W and concentration of 1.0 M (Figure S3). As expected, the use of a 400 W lamp tripled the productivity of the reaction in comparison to the 125 W results. The reaction tolerates the higher concentration of 1.0 M but a minor decrease in productivity was observed.

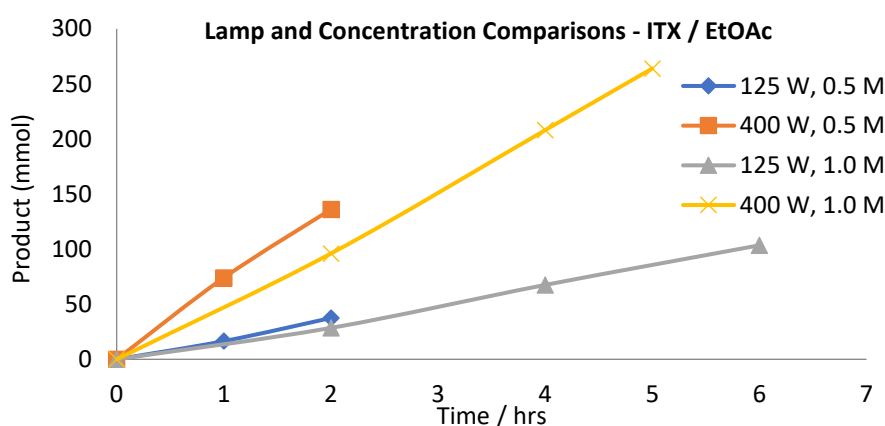
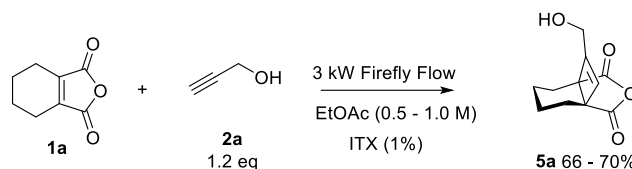


Figure S3: Lamp power comparisons for 125 W (150 ml) and 400 W (400 ml) in EtOAc (0.5 – 1.0 M)

2.1.4. Transfer to Large Scale Continuous Flow Reactor with a 3 kW Lamp – Predicting the Flow Rate From Batch Results

The flow reactor (Firefly) used here has been described before and was used without any deviation from the description in the reference.^[1]



Scheme S1: THPA / PA [2+2] with Firefly parallel tube flow reactor

The Firefly at 3 kW was previously shown to give 10× productivity of a 400 W reactor. The solution in the 400 W, 400 ml batch reactor took 2 hrs to reach full conversion at 0.5 M giving an ‘*effective flow rate*’ of 3.3 ml/min. A likely optimal flow rate is therefore around 33 ml/min. In practice the reaction could be run at 36 ml/min at nearly full conversion.

The productivity for the 1.0 M reaction was slightly reduced and the 400ml solution took 5 hrs to reach full conversion. This gives an ‘*effective flow rate*’ of 1.3 ml/min and a predicted 3 kW firefly flow rate of 13 ml/min. The experimental results were in agreement with this as demonstrated by a 0.5 mole trial run.

0.5 M, 36 ml/min, 64% = **691 mmol/hr**

0.5 M, 25 ml/min, 65% = **488 mmol/hr**

1.0 M, 16 ml/min, 64% = **616 mmol/hr**

500 mmol (500 ml run) – 76 g THPA

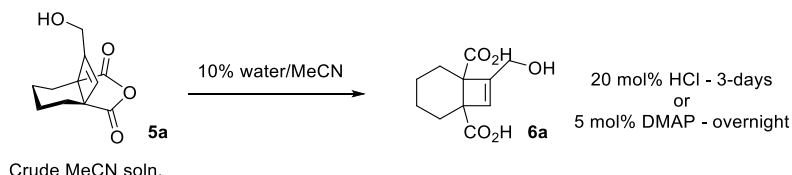
1.0 M, 13 ml/min, 66% = **515 mmol/hr**



For the following large (1 mole +) scale demonstrations, the operational conditions of 0.5 M and 30 ml/min were chosen to give the greatest levels of confidence the reaction would remain at full conversion for the duration of the reaction.

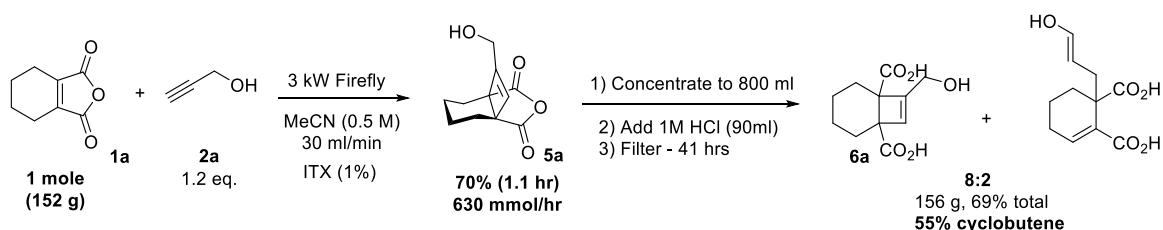
2.2. Homogenous Lactone Hydrolysis Investigation in Batch

The addition of 1 M HCl aq. (10% vol) to a crude MeCN (0.5 M) reaction mixture led to the slow hydrolysis over a period of 3 days (Scheme S2). The hydrolysis rate did not appear to be significantly increased by simply heating the reaction. The diacid product precipitated out and could be filtered off in reasonable yield. The addition of DMAP to 10% water in MeCN resulted in a faster hydrolysis but the product did not precipitate out, even after acidifying with HCl.



Scheme S2: Hydrolysis of [2+2] product anhydride

The photochemistry / MeCN hydrolysis sequence was performed on a 1 mole scale with the Firefly at 3 kW (0.5 M, 30 ml/min) to provide diacid for ring opening studies in batch and with the high temperature water flow reactor (Scheme S3).



Scheme S3: Photochemical [2+2] / hydrolysis sequence on 1 mole scale

Prior to hydrolysis, the reaction mixture was concentrated from 2 L to 800 ml before the addition of 1M HCl. The product was isolated, along with the hydrolysed by-product of the photochemical step, by filtration (Figure S4).

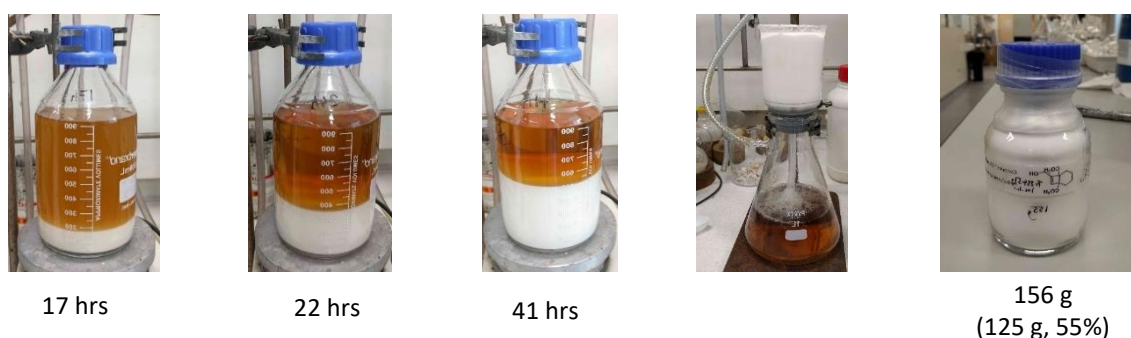
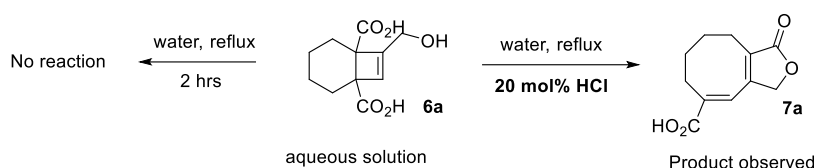


Figure S4: Slow, room temperature hydrolysis of 1 mole scale crude, concentrated photosylate (MeCN)

2.3. Biphasic Lactone Hydrolysis / Aqueous Ring Opening Sequence

As an alternative approach to hydrolysis, the crude EtOAc solution was stirred as an emulsion with water. Unlike the MeCN / water hydrolysis, the reaction rate could be increased with heating such that it was at full conversion within 1 hr at 60°C. Since the hydrolysed diacid product was formed as an aqueous solution, this method relies on the electrocyclic ring opening to be carried out in water. Before further optimization, the thermal ring-opening step was investigated.

No significant reaction was observed on heating an aqueous solution at reflux for 2 hours. The addition of catalytic HCl to the aqueous solution successfully accelerated the reaction at reflux and pleasingly, the product precipitated out in high purity after the solution was cooled (Scheme S4).



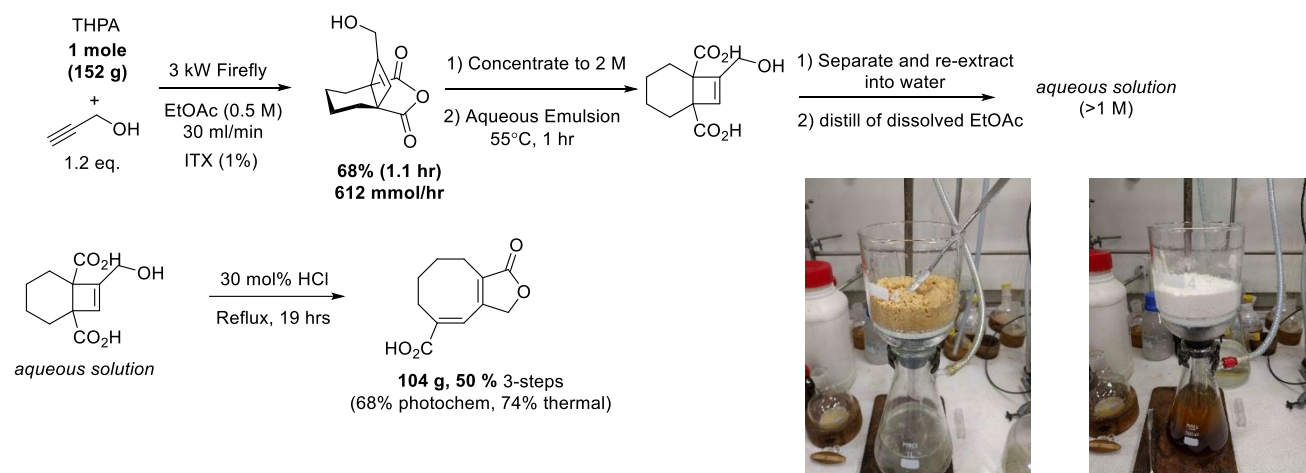
Scheme S4: Novel acid catalyzed ring opening of cyclobutene diacid in aqueous solution

In further trial reactions it was found that any significant residual EtOAc dissolved in the aqueous was hydrolyzed to AcOH and EtOH and had the effect of inhibiting the reaction and making purification more difficult. The best results were obtained when excess EtOAc was distilled from the aqueous solution using a rotary evaporator.

2.4. Initial Linking of Flow Photochemical and Batch Thermal Reactions

2.4.1. 1 Mole Scale Photo/Thermal Reaction Sequence

The optimized reaction sequence was run through on a mole scale to demonstrate the potential for further scale-up (Scheme S5). The photochemistry proceeded at full conversion to give about 70% of the cyclobutene. The addition of hexane (200 ml) to the concentrated photosylate (700 ml) assisted with the separation and allowed the hydrolysed diacid product to be extracted into the aqueous solution more efficiently.

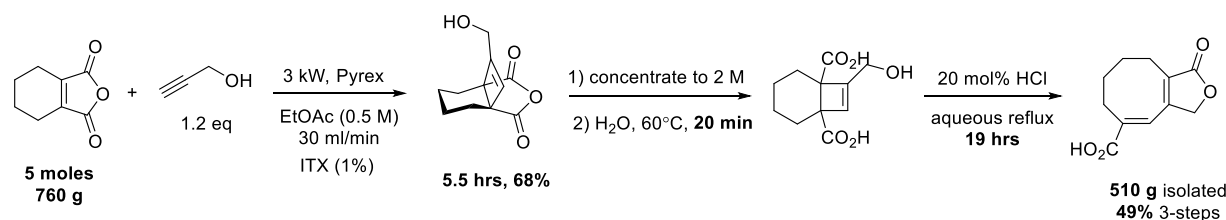


Scheme S5: Trial 1 mole scale flow [2+2] photochemistry / hydrolysis / aqueous electrocyclic ring opening

After heating at reflux in acidified aqueous solution, a clumpy suspension of product formed which was filtered to give a soft yellow solid. This was filtered with diethyl ether to give pure product as a free-flowing colourless powder 104 g, 50% - (68% photochem, 74% thermal)

2.4.2. 5 Mole Scale Photo/Thermal Reaction Sequence

With increased confidence in the optimized conditions, the reaction sequence was repeated on a 5 mole scale to investigate the robustness of the procedure (Scheme S6).



Scheme S6: 5 mole scale flow [2+2] photochemistry / hydrolysis / aqueous electrocyclic ring opening

The photochemical reaction solution was prepared (10 L, 0.5 M, EtOAc) in two 5 L bottles. Each bottle contained THPA (380 g, 2.5 mol) and propargyl alcohol (175 ml, 3 mol) and made up to 5 L volume in EtOAc. The solvent was used as purchased with minimal degassing prior to use by stirring under reduced pressure during THPA addition. Full conversion to product was observed for the duration of the flow reaction, which took just over 5.5 hours at 30 ml/min (Figure S5, left) with the Firefly parallel

tube flow reactor with Pyrex filter and Hg lamp at 3 kW. This indicates there was no fouling of the reaction tubing due to deposition of degradation by-products.

The photosylate was concentrated to 2.5 L and hydrolyzed by forming an emulsion with water (1.4 L) and hexane (700 ml) at 60°C for 20 mins with an overhead stirrer in a 5 L Radleys Reactor-Ready double jacketed vessel (Figure S5, right). Separation and re-extraction with water (1 L) gave an aqueous solution of the diacid from which dissolved EtOAc was removed by distillation under reduced pressure to give a volume of approximately 3 L.

The aqueous solution was further diluted with water (500 ml) and heated under reflux conditions with the 5 L Radleys Reactor-Ready with 1 mole (83 ml, 12 M) of HCl. Conversion to the ring-opened product was measured by $^1\text{H-NMR}$ to be 92% after 18 hours. The mixture was cooled after 19 hours before filtering the precipitated product and washing with water, MeOH and Et₂O to give the product as a powder (510 g, 49% overall, see Figure S6).



Figure S5: *left* – 5 mole scale irradiation of THPA with Firefly flow reactor; *right* – 5 mole scale hydrolysis as an emulsion



Figure S6: *left* – final filtration of 5 mole scale reaction; *right* – product batches accumulated during studies

3. High Temperature Water (HTW) Reactor Set-ups

3.1. Reactor Description and Details

3.1.1. Large Scale Thermal Flow Reactor

Large scale continuous flow reactions were carried out using a custom-built flow system constructed primarily from stainless steel Swagelok tubing and fittings, a schematic of which can be seen in Figure S7, below. The system in brief is made up of two HPLC pumps, a heated coil reactor with an internal volume of 43.7 ml, a pipe-in-pipe cooling jacket and a manual back pressure regulator (BPR). The heated reactor consists of a 6 m coil of 1/4" OD Swagelok tubing formed around an aluminium heating block, which contains a cartridge heater and is surrounded by an additional band heater. An optional third pump, which can act as a quench to rapidly cool and dilute the reactor outflow is also present. The system temperature is controlled by a Eurotherm heater controller, attached to the reactor and monitored by four K-type thermocouples, two within the heating block and two in flow, downstream of the reactor and the upstream of the BPR. Reagents are introduced to the system via up to three Gilson 305 HPLC pumps, fitted with 5, 10 or 25 SC pump heads depending on the desired flow rate. The system pressure is set by a TESCO manual BPR (26-1700 series) and monitored by three RDP electronics pressure transducers located in flow, just downstream of each pump. A trip system connected to the equipment which isolates power to the pumps and heaters in case of an over-pressure or over-temperature, being recorded in the system and a Swagelok sprung relief valves provides additional overpressure protection.

Care must be taken when designing or working with high pressure continuous flow systems and solvents above their boiling points due to the high temperature, pressure and the potential for high temperature vapours to be released potential causing severe burns. The temperature and pressure ratings of rig components must not be exceeded. The flammability and reactivity of solvents used should also be considered particularly at elevated temperature and pressure, the autoignition temperature must not be exceeded and reactions carried out below these conditions with a safe margin.

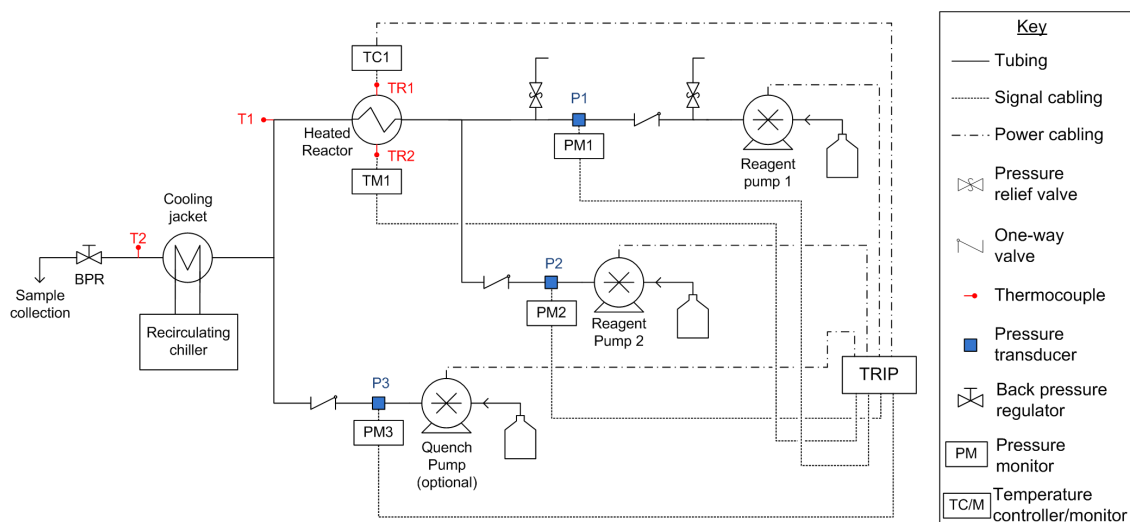


Figure S7. Rig diagram for the large-scale continuous flow thermal reactor, showing the positions of and connections between major rig components. Stainless steel tubing is indicated by a solid line, dotted lines show the overtemperature and overpressure inputs to the trip system and dashed lines indicate equipment controlled by the trip system, power to which is disconnected should the trip activate.

3.1.2. Small Scale Thermal Flow Reactor

To allow a broader range of substrates to be investigated, a smaller scale thermal reactor and set-up were constructed (Figure S8). This design of this system was similar to that described above, but scaled down to suit a 3 m long coiled reactor constructed from 1/16" OD Swagelok tubing, with an internal volume of 0.77 ml. This gave a total rig volume of less than 2 ml, including reagent feed lines, of which around 1.2 ml is pressurised. Jasco PU-980 HPLC pumps and BP-2080 Back pressure regulator were used in the small scale set-up to suit the lower flow rates required, while needle valves fitted upstream of the pumps allow them to be primed without depressurising the entire system.

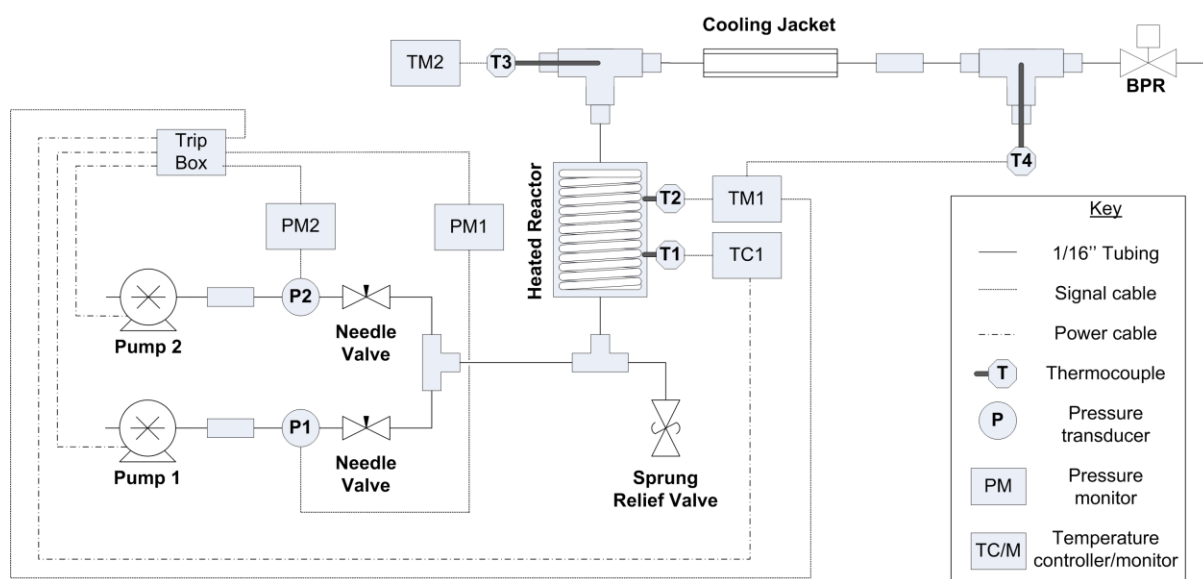


Figure S8. Rig diagram for the small scale continuous flow thermal reactor, showing the positions of and connections between major rig components. Stainless steel tubing is indicated by a solid line, dotted lines show the overtemperature and overpressure inputs to the trip system and dashed lines indicate equipment controlled by the trip system, power to which is disconnected should the trip activate.

3.1.3. Standard Operating Procedure for Thermal Flow Reactors

A typical continuous flow thermal reaction procedure follows. The standard operating procedures of each size of reactor are the same, with the exceptions of the equilibration periods, priming techniques and method of setting back pressure. For the larger reactor, the minimum equilibration period was taken as the time for three reactor volumes worth of solution to be pumped into the reactor, however this was increased to two total rig volumes for the smaller reactor (>5 reactor volumes), to allow for the increased proportion of non-reactor volume within the system.

Start-up

1. Switch on power to system and reset trip. Pressure monitors, temperature monitors, back pressure regulator (BPR) and cooling bath should turn on immediately, pumps and heater should turn on once the trip is reset.
2. Check temperature and pressure trips are set to the correct value.
3. Prime pump(s) using desired reaction solvent. Ensure there is no air in the pump feed lines and the pumps are working efficiently.
4. Once solvent is flowing out of the rig, set the system pressure using the BPR.
5. Check for leaks. If any leaks are found, the system pressure should be reduced to ambient and the fitting re-seated and tightened/replaced as necessary.
6. Turn on cooling bath if used.
7. Turn on heater controller (TC1), set heater temperature, typically 250 °C, and allow reactor temperature to stabilise.

Reaction

8. Switch pump feeds to reagents and set pump flow rates as desired.
9. Wait time for equilibrium.
10. Collect sample(s).
11. If multiple samples are to be collected at different conditions, make the necessary changes and repeat equilibrium and sampling process until all samples are collected.

Shutdown

12. Substitute solvent for the reagent feeds.
13. Flush reactor at temperature until outflow of system is colourless.
14. Set heaters to zero.
15. Allow system to cool until system is below the boiling point of the solvent in use.
16. Slowly release pressure at BPR, then stop pumps.
17. Turn off system.

To account for minor fluctuations in rig conditions, all samples were collected in triplicate. Once collected, a known volume of each sample was dried under reduced pressure, before biphenyl was added as an external standard and the samples submitted for ^1H NMR in deuterated DMSO.

3.1.4. Batch Thermal Reactions

Initial thermal screening reactions were carried out in a series of stainless steel autoclaves with an internal volume of 10 ml, the design of which has been published previously.^[2]

This reaction set-up allows small scale reactions to be carried out at above the boiling point of the solvents, as the sealed reactors are pressurised autogenously, while attached temperature and pressure monitoring allow the reaction conditions to be monitored throughout. The reaction set-up in brief composes of two wells, one heated and the other water cooled, and the autoclaves can be moved between the wells without interrupting the pressure or temperature monitoring.

The desired reactants and solvent are loaded into a stainless steel autoclave, and the autoclave is sealed, before being placed into either well as required. Short reaction times are possible, as the combination of pre-heating the thermal well and efficient heat transfer to the relatively small reaction vessels allow the reactants to reach the desired temperatures (typically 200-300 °C) in around 7 minutes. The reactants are then held at the desired temperature for 10 minutes (timer started once the reaction temperature is within 5 °C of target), before the autoclave is transferred to the water cooled well, and the temperature rapidly decreased. Full cooling of the reactors takes around 10 minutes, although the internal temperature typically decreases by half within the first 2 minutes.

3.2. Photochemical Flow Reactor linked with HTW Reactor

3.2.1. Photochemical Set-up

FEP coil reactors,^[3] similar to those previously described, were used to carry out the photochemical step of these reactions in flow. These reactors consist of one or more layers of thin walled FEP tubing coiled around a central light source. For the initial photochemical flow reactions, FEP tubing (2.7 mm ID 3.1 mm OD, supplied by Adtech) was coiled in a single layer around a borosilicate cylinder into which a quartz immersion wells sized to fit 400 W medium pressure mercury arc lamps, was placed (all glassware and lamps supplied by Photochemical Reactors LTD.). This reactor had an irradiated volume of 75 ml. A Masterflex peristaltic pump with PTFE pump head was then used to flow the photochemical reagents in acetonitrile through the reactor.

To ensure safe containment of the UV lamps, each reactor was wrapped in aluminium foil to minimise stray light, and opaque shields were placed in front of the reactors. Due to the possibility of ozone generation, photochemical reactors were only run inside appropriately extracted boxes. Lamp cooling was provided by a recirculating cooling bath, filled with water and operated at 15 °C. A low-flow cut-off device, supplied by Photochemical Reactors LTD, was used to ensure sufficient cooling flow was maintained throughout. Thin K type thermocouples inserted between the immersion well and the inner layer of FEP tubing allowed reaction temperatures to be estimated.

To ensure that any samples collected were representative of equilibrium conditions, the UV lamps were allowed to reach temperature (with cooling flowing) for 30 minutes before the photochemical reactions were started. Likewise, a minimum of two reactor volumes worth of reagents were pumped before samples were taken. All samples were collected in triplicate and a known volume of each

sample was dried under a flow of nitrogen, before biphenyl was added as an external standard and the samples submitted for ^1H NMR in deuterated acetonitrile.

To allow scale-up of the daisychain process, three double layer reactors, coiled around quartz immersion wells sized to fit 400 W medium pressure mercury arc lamps, with an inner borosilicate filter placed between the lamp and the immersion well in each case reactors were used. These reactors had an average irradiated volume of 132 ml, and were connected in parallel, with a separate pump feeding each reactor. The combined outflows of which provided the inlet stream of the thermal reactor.

3.2.2. Linking of the Photochemical Flow reactor with the HTW Reactor

To allow the photochemical and thermal steps of this reaction to be combined into a single continuous flow operation, a daisy-chained system was developed, see main text Figure 2. Up to three FEP coil reactors, operating in parallel, were fitted upstream of the thermal system described above, with the outflow of each photoreactor combined to provide the reagent feed for the thermal reactor.

3.2.3. Batch Photochemical Reactions

Batch photochemical reactions were carried out in a commercially available 100 ml borosilicate immersion well reactor, surrounding a 125 W medium pressure mercury arc lamp.

4. Optimisation of Thermal Reaction in High Temperature Water

4.1. Batch Ring Expansion/Lactonization of 6a in High Temperature Water/Acetonitrile Mixtures

Batch synthesis of **7a** ((*E*)-1-oxo-1,3,6,7,8,9-hexahydrocycloocta[c]furan-5-carboxylic acid) from **6a** (7-(hydroxymethyl)bicyclo[4.2.0]oct-7-ene-1,6-dicarboxylic acid) in high temperature water and high temperature water containing solvent mixtures.

Standard Procedure

Diacid **6a** (57 mg, 0.25 mmol) and solvent (water or water/acetonitrile mixture, 5 ml) was added to stainless steel autoclave. The autoclave was then sealed, heated and held at the reaction temperature for 10 minutes, before being rapidly water cooled. Once fully cooled the contents of the reactor were transferred to a measuring cylinder to check for any loss of solvent, which may indicate a reactor leak, before sampling. For reactions in water where precipitation of the product occurred, samples were either filtered to obtain the pure product or made up to a known volume with acetone before a subsample was dried under reduced pressure and biphenyl added as an external standard to allow semi-quantitative ^1H NMR analysis (Table S2).

Table S2: The effect of reaction temperature on batch electrocyclic ring opening reactions in HTW

Solvent	Reaction temperature (°C)	Yield of ring opened product (%)	Conversion of diacid (%)
Water	100	0	0
Water	120	0	0
Water	140	5	5
Water	160	22	22
Water	180	60	65
Water	200	99	Full
Water	220	81	Full
Water plus trace ethyl acetate	200	87	Full
50:50 Water:Acetonitrile	200	94	Full

Using pure water as the solvent, full conversion and near quantitative yields were achieved for the 10 minute reaction at 200 °C, the reaction did not reach completion within the 10 minute reaction time below this temperature and some decomposition of the product was observed at 220 °C. Even trace quantities of ethyl acetate within the solvent mixture, lead to an appreciable drop in yield, and increase in reaction pressure. Near equivalent yields to pure water were observed at 200 °C when using a 50:50 v/v mixture of acetonitrile and water, and the reaction products remained in solution even after cooling.

4.2. Continuous Flow Ring Expansion/Lactonization of **6a** in High Temperature Water/Acetonitrile Mixtures

Continuous flow synthesis of **7a** ((E)-1-oxo-1,3,6,7,8,9-hexahydrocycloocta[c]furan-5-carboxylic acid) from **6a** (7-(hydroxymethyl)bicyclo[4.2.0]oct-7-ene-1,6-dicarboxylic acid) in high temperature water and high temperature water containing solvent mixtures. These reactions were carried out in the larger of the thermal reactors, and followed the standard operating procedure described above (Table S3).

Table S3: Screening continuous flow conditions for electrocyclic ring opening of **6a** to **7a** in HTW

Temperature (°C)	Flow rate (ml/min)	Solvent ratio (H ₂ O:ACN)	Yield ¹ H NMR (isolated) (%)	Conversion (%)
200	3.8	100:0	68	93
200	5.1	100:0	66	84
200	7.6	100:0	55	68
200	15.2	100:0	33	38
210	7.5	50:50	81	88
220	7.4	50:50	95	95
200	8	25:75	44 (42)	52
220	8	25:75	85 (79)	89
220	16	25:75	75	73
220	18	25:75	61	58
240	16	25:75	83	87
260	16	25:75	92	92

For the reactions carried out in water, the reactor temperature was set to 200 °C and pressure to 100 bar, a 0.05 M starting solution of diacid in water was introduced to the reactor, at the flow rates shown and an additional water feed at the same flow rate was introduced via the quench pump downstream of the reactor, to dilute the outflow and minimise the accumulation of solid within the reactor due to precipitation of **7a** although a large volume of solid was subsequently removed from the reactor post reaction, indicating product accumulation had occurred and potentially explaining the lower than predicted yields.

For reactions in acetonitrile water mixtures, the system pressure was 100 bar, reagent concentrations of 0.06 M of diacid made up in the appropriate solvent mixture were used at the flow rate shown, and no quench pump was required, as reagents and products remained in solution. Isolated yields were obtained for two sets of conditions, via removal of the acetonitrile under reduced pressure and filtration, showing good agreement with yield obtained by NMR, and excellent purity.

4.3. Continuous-Flow Combined Hydrolysis and Ring Opening

Combined hydrolysis and ring opening of **5a** (8-(hydroxymethyl)-4,5,6,7-tetrahydro-1H,3H-3a,7a-ethenoisobenzofuran-1,3-dione) to **7a** ((*E*)-1-oxo-1,3,6,7,8,9-hexahydrocycloocta[c]furan-5-carboxylic acid).

Combined hydrolysis and ring opening reaction in batch indicated full conversion of the photoproduct **5a** (0.05M in 5 ml solvent) and at least 95% yield of **7a** were obtained in a 10 minute reaction at 200 °C for solvent mixtures containing a minimum of 25% water. Below this percentage diacid **6a** was recovered in addition to **7a**.

Similar yields were obtained when using crude photoproduct (approx. 0.06 M of **5a** in acetonitrile) diluted with the appropriate volume of water. In this case additional peaks believed to correspond to the hydrolysis products of non-bridged photoproduct **4a** and any remaining propargyl alcohol were also observed via NMR.

For reactions carried out in continuous flow, crude photochemical solutions were used (containing approx. 0.06M of **5a** in acetonitrile) and the optimal solvent ratio was found to be 50:50 acetonitrile to water, which was found to increase the rate of hydrolysis. A higher pressure of 150 bar was used to minimise expansion of the higher volatility solvent mixture. Two pumps were used to generate the required solvent mixture in situ, with matched flow rate of water introduced by pump 1 and photoproduct in CH₃CN introduced via pump 2.

Table S4: Screening continuous flow conditions for combined hydrolysis / electrocyclic ring opening of **5a** to **7a** in HTW

Starting material	Temperature (°C)	Flow rate (ml/min)	Water (%)	Acetonitrile (%)	Yield of ring opened product (%)	Yield of diacid (%)	Conversion (%)
5a	200	Batch	100	0	95	0	Full
5a	200	Batch	50	50	95	0	Full
5a	200	Batch	25	75	95	0	99
5a	200	Batch	10	90	35	40	78
5a	200	Batch	5	95	23	40	64
5a	200	Batch	0	100	7	0	28
Crude	200	Batch	50	50	94	0	Full
Crude	260	34	50	50	95	1	Full

5. Batch Photochemistry of Additional Substrates

Batch photochemical reactions were carried out in a 100 ml borosilicate immersion well photoreactor, fitted with a water cooled 125 W Hg arc lamp, all obtained from Photochemical Reactors LTD. Prior to irradiation, solutions were degassed by passing a flow of nitrogen through the solution for 15 minutes.

8-(2-hydroxyethyl)-4,5,6,7-tetrahydro-1*H*,3*H*-3a,7a-ethenoisobenzofuran-1,3-dione (**5b**)

A solution of 3,4,5,6 tetrahydrophthalic acid anhydride (1.52 g, 10 mmol) and 3-butyne-1-ol (0.76 ml, 10 mmol) in acetonitrile (100 ml) was irradiated for 3 hours. Half of the solution (50 ml) was retained without further purification for reactions using the crude photochemical product. The solvent was removed from the remaining 50 ml of photochemical reaction mixture under reduced pressure and flash chromatography of the residue (0-50% EtOAc/Heptane) afforded the title compound as a pale yellow oil (0.82 g, 74%); (*R*_f 0.28, 50% EtOAc/Heptane). Further elution gave 2-(3'-hydroxy-1'-butenyl)-2,3,4,5-tetrahydrothalic anhydride (**4b**) as a pale yellow oil (0.14 g, 12%); (*R*_f 0.18, 50% EtOAc/Heptane).

7-(hydroxymethyl)-5,6-dihydro-1*H*,3*H*,4*H*-3a,6a-ethenocyclopenta[*c*]furan-1,3-dione (**5c**)

A solution of 1-cyclopentene-1,2dicarboxylic anhydride (0.95 g, 6.9 mmol) and propargyl alcohol (0.42 ml, 6.9 mmol) in acetonitrile (100 ml) was irradiated for 3 hours. This yielded a solution containing the title compound in 79% yield via ¹H NMR against a biphenyl external standard which was used for thermal reactions without further purification.

8-(hydroxymethyl)-9-methyl-4,5,6,7-tetrahydro-1*H*,3*H*-3a,7a-ethenoisobenzofuran-1,3-dione (**5d**)

A solution of 3,4,5,6 tetrahydrophthalic acid anhydride (1.52 g, 10 mmol) and 2-butyne-1-ol (0.75 ml, 10 mmol) in acetonitrile (100 ml) was irradiated for 4 hours. This yielded a solution containing the title compound in 73% yield via ¹H NMR against a biphenyl external standard which was used for thermal reactions without further purification.

6. Optimisation of Small Scale Thermal Reactor for the Ring expansion of **5b** and **5c**.

Continuous flow synthesis of (E)-1-oxo-3,4,7,8,9,10-hexahydro-1H-cycloocta[c]pyran-6-carboxylic acid (**7b**) from purified and crude photoproduct (**5b**)

These reactions were carried out in the smaller of the thermal reactors, and followed the standard operating procedure described above. Reactions carried out at 150 bar using either purified **5b** (70 mM in acetonitrile) or crude photochemical solutions (containing approx. 70 mM of **5b** in acetonitrile). Similar results were obtained in either case. Two pumps were used to generate the required solvent mixture in situ, with matched flow rate of water introduced by pump 1 and photoproduct in acetonitrile introduced via pump 2. Flow rates quoted are the total flow rate, calculate as a sum of all water and acetonitrile flow rates. Yields were obtained via ¹H NMR against a biphenyl external standard and calculated based on an average of two samples, normalised against a measured starting material sample, and were corrected for dilution, pump efficiency and sample evaporation during collection. > 95% conversion of the starting anhydride was observed in each case.

Table S5: Screening continuous flow conditions for formation of **7b** from **5b**

Substrate	Temperature (°C)	Flow rate (ml/min)	ACN:H ₂ O ratio	Diacid yield (%)	Ring opened yield (%)
Purified	200	0.4	1:1	51	25
Purified	225	0.4	1:1	17	57
Purified	250	0.2	1:1	0	62
Purified	250	0.4	1:1	0	61
Crude	200	0.2	1:1	28	28
Crude	200	0.4	1:1	66	26
Crude	200	0.8	1:1	84	15
Crude	225	0.2	1:1	5	59
Crude	225	0.4	1:1	22	54
Crude	225	0.8	1:1	55	43
Crude	250	0.4	1:1	3	61
Crude	250	0.6	1:1	7	60
Crude	250	0.8	1:1	11	50
Crude	260	0.4	1:1	0	49
Crude	260	0.8	1:1	8	57
Crude	260	1.2	1:1	18	48
Crude	250	0.4	3:5	0	57
Crude	250	0.4	5:3	14	50

Continuous flow synthesis of 1-oxo-3,6,7,8-tetrahydro-1H-cyclohepta[c]furan-5-carboxylic acid (**7c**) from crude photoproduct (**5c**)

These reactions were carried out in the smaller of the thermal reactors, and followed the standard operating procedure described above. Reactions carried out at 150 bar using crude photochemical solutions, which were diluted with acetonitrile to improve solubility giving 33mM concentrations of **5c**. Two pumps were used to generate the required 1:1 solvent mixture in situ, with matched flow rate of water introduced by pump 1 and photoproduct in acetonitrile introduced via pump 2. Flow rates quoted are the total flow rate, calculate as a sum of all water and acetonitrile flow rates Yields were

obtained via ^1H NMR against a biphenyl external standard and calculated based on an average of two samples, normalised against a measured starting material sample, and were corrected for dilution, pump efficiency and sample evaporation during collection. Greater than 95% conversion of the starting anhydride was observed in each case. * indicates evidence of acetonitrile hydrolysis during reaction or conditions likely to result in sure hydrolysis.

Table S6: Screening continuous flow conditions for formation of **7c** from **5c**

Temperature (°C)	Flow rate (ml/min)	Diacid yield (%)	Ring opened yield (%)
200	0.4	95	0
225	0.4	Quant.	0
250	0.4	48	28
260	0.4	36	45
260	0.2	14	53
250	0.2	26	39
250	0.1	9	41
235	0.1	38	41
235	0.04	3	9
280*	0.4	4	50
280*	0.8	20	48
300*	0.8	2	72
300*	1.2	9	78
320*	1.2	0	62
320*	1.6	1	66

Continuous flow thermal reaction of 8-(hydroxymethyl)-9-methyl-4,5,6,7-tetrahydro-1H,3H-3a,7a-ethenoisobenzofuran-1,3-dione (**5d**)

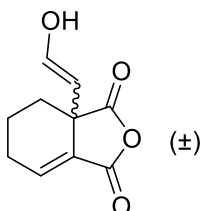
These reactions were carried out in the smaller of the thermal reactors, and followed the standard operating procedure described above. Reactions carried out at 150 bar using crude photochemical solutions (containing approx. 64 mM of **5d** in acetonitrile). Two pumps were used to generate the required 1:1 solvent mixture in situ, with matched flow rate of water introduced by pump 1 and photoproduct in acetonitrile introduced via pump 2. Flow rates quoted are the total flow rate, calculate as a sum of all water and acetonitrile flow rates Yields were obtained via ^1H NMR against a biphenyl external standard and calculated based on an average of two samples, normalised against a measured starting material sample, and were corrected for dilution, pump efficiency and sample evaporation during collection. * indicates evidence of acetonitrile hydrolysis during reaction or conditions likely to result in such hydrolysis.

Table S7: Screening continuous flow conditions for thermolysis of **5d**

Reaction temperature (°C)	Total flow rate (ml/min)	Diacid yield 6d (%)	Yield 8 (%)	Yield 9 (%)
250	0.8	68	4	0
275*	0.4	20	10	25
275*	0.8	45	5	15
300*	0.4	9	12	34
300*	0.8	35	11	31
300*	1.2	45	9	21

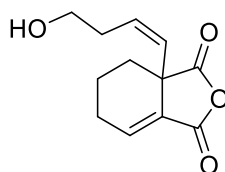
7. Characterization Data

Compounds **4a-b**, **5a-d**, **6a** and **7a** were prepared in agreement with data reported in the literature.



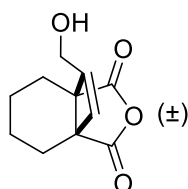
(4a) (*E*)-3a-(3-hydroxyprop-1-en-1-yl)-3a,4,5,6-tetrahydroisobenzofuran-1,3-dione^[4]

¹H NMR (400 MHz, CDCl₃, 25 °C, TMS): δ =7.13 (t, *J*=3.7 Hz, 1H, CH), 5.75 (d, *J*=15.6 Hz, 1H, CH), 5.70 (dt, *J*=15.6, 3.5 Hz, 1H, CH), 4.18 (d, *J*=3.5 Hz, 2H, CH₂), 3.75 (br, 1H, OH), 2.50-2.22 (m, 2H, CH₂), 2.19-2.13 (m, 1H, CH_{2A}), 1.89-1.54 (m, 3H, CH₂ + CH_{2B}); ¹³C NMR (100 MHz, CDCl₃, 25 °C, TMS): δ =172.0 (CO), 163.4 (CO), 142.1 (CH), 135.6 (CH), 128.5 (C), 128.3 (CH), 62.4 (CH₂), 50.2 (C), 27.4 (CH₂), 25.3 (CH₂), 16.5 (CH₂).



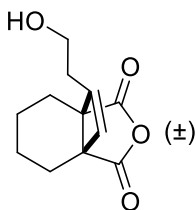
(4b) 2-(3'-hydroxy-1'-butenyl)-2,3,4,5-tetrahydrothalic anhydride^[4]

¹H NMR (400 MHz, CDCl₃, 25 °C, TMS): δ =7.07 (t, *J*=3.6 Hz, 1H, CH), 5.53-5.49 (m, 2H, 2x CH), 4.85 (b, 1H, OH), 3.58 (td, *J*=6.5, 1.2 Hz, 2H, CH₂), 2.44-2.18 (m, 4H, 2x CH₂), 2.10-2.04 (m, 1H, CH_{2A}), 1.82-1.56 (m, 2H, CH₂), 1.55-1.46 (m, 1H, CH_{2B}); ¹³C NMR (100 MHz, CDCl₃, 25 °C, TMS): δ =172.2 (CO), 163.5 (CO), 142.3 (CH), 133.4 (CH), 129.8 (CH), 128.1 (C), 61.4 (C), 50.3 (C), 35.3 (CH₂), 27.2 (CH₂), 25.2 (CH₂), 16.2 (CH₂).



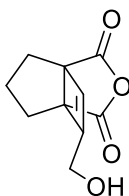
(5a) 8-(hydroxymethyl)-4,5,6,7-tetrahydro-1*H*,3*H*-3a,7a-ethenoisobenzofuran-1,3-dione^[5]

¹H NMR (400 MHz, CDCl₃, 25 °C, TMS): δ =6.28 (t, *J*=1.8 Hz, 1H, CH), 4.20 (d, *J*=1.8 Hz, 2H, CH₂), 3.32 (b, 1H, OH), 2.10-1.94 (m, 4H, 2x CH₂), 1.68-1.56 (m, 2H, CH₂), 1.54-1.41 (m, 2H, CH₂); ¹³C NMR (100 MHz, CD₃CN, 25 °C, TMS): δ =173.8 (CO), 172.8 (CO), 155.9 (C), 134.4 (CH), 58.2 (CH₂), 54.5 (C), 51.8 (C), 25.3 (CH₂), 24.5 (CH₂), 19.7 (CH₂), 19.6 (CH₂).



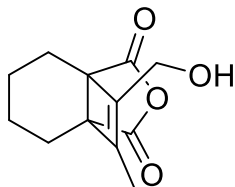
(5b) 8-(2-hydroxyethyl)-4,5,6,7-tetrahydro-1*H*,3*H*-3*a*,7*a*-ethenoisobenzofuran-1,3-dione^[5]

¹H NMR (400 MHz, CDCl₃, 25°C, TMS): δ =6.17 (t, *J*=1.7 Hz, 1H, CH), 3.74 (td, *J*=6.3, 1.7 Hz, 2H, CH₂), 2.46 (b, 1H, OH), 2.45-2.29 (m, 2H, CH₂), 2.08-1.89 (m, 4H, 2xCH₂), 1.67-1.54 (m, 2H, CH₂), 1.53-1.39 (m, 2H, CH₂); ¹³C NMR (100 MHz, CDCl₃, 25 °C, TMS): δ =172.65 (CO), 172.63 (CO), 153.8 (CH), 135.0 (C), 59.0 (CH₂), 54.7 (C), 51.1 (C), 31.4 (CH₂), 25.2 (CH₂), 24.1 (CH₂), 19.5 (CH₂), 19.3 (CH₂); HRMS (ESI) *m/z* [M+H]⁺ calcd for C₁₂H₁₅O₄: 223.0965, found: 223.0955.



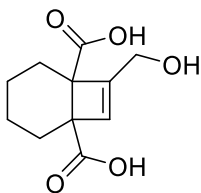
(5c) 7-(hydroxymethyl)-5,6-dihydro-1*H*,3*H*,4*H*-3*a*,6*a*-ethenocyclopenta[*c*]furan-1,3-dione^[4]

¹H NMR (400 MHz, (CD₃)₂SO, 25°C, TMS): δ =6.26 (t, *J*=1.9 Hz, 1H, CH), 5.13 (b, 1H, OH), 4.05 (dd, *J*=16.2, 1.9 Hz, 1H, CH_{2A}), 3.96 (dd, *J*=16.2, 1.6 Hz, 1H, CH_{2B}), 2.10-1.82 (m, 5H, 2x CH₂ + CH_{2A}), 1.74-1.68 (m, 1H, CH_{2B}).



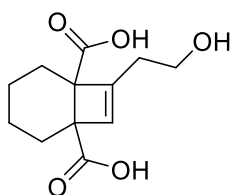
(5d) 8-(hydroxymethyl)-9-methyl-4,5,6,7-tetrahydro-1*H*,3*H*-3*a*,7*a*-etheno-isobenzofuran-1,3-dione^[5]

¹H NMR (400 MHz, CDCl₃, 25°C, TMS): δ =4.24 (q, *J*=1.3 Hz, 2H, CH₂), 2.44 (b, 1H, OH), 2.09-2.01 (m, 2H, CH₂), 1.98-1.91 (m, 2H, CH₂), 1.82 (t, *J*=1.3 Hz, 3H, CH₃), 1.67-1.45 (m, 4H, 2x CH₂); ¹³C NMR (100 MHz, CDCl₃, 25 °C, TMS): δ =172.9 (CO), 172.1 (CO), 145.4 (C), 144.2 (C), 57.0 (CH₂), 53.1 (C), 52.1 (C), 24.5 (CH₂), 23.7 (CH₂), 19.74 (CH₂), 19.71 (CH₂), 11.3 (CH₃); HRMS (ESI) *m/z* [M+Na]⁺ calcd for C₁₂H₁₄NaO₄: 245.0784, found: 245.0783.



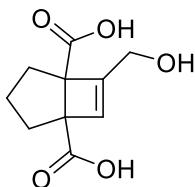
(6a) 7-(hydroxymethyl)bicyclo[4.2.0]oct-7-ene-1,6-dicarboxylic acid^[6]

¹H NMR (400 MHz, (CD₃)₂CO, 25°C, TMS): δ=10.56 (b, 2H, OH), 6.11 (app. t, *J*=1.8 Hz, 1H, CH), 4.24 (dd, *J*=15.3, 1.8 Hz, 1H, CH_{2A}), 4.16 (dd, *J*=15.3, 1.6 Hz, 1H, CH_{2B}), 3.00 (b, 1H, OH), 2.20-2.09 (m, 2H, CH₂), 1.92-1.85 (m, 1H, CH_{2A}), 1.80-1.72 (m, 1H, CH_{2B}), 1.65-1.54 (m, 4H, 2x CH₂); ¹³C NMR (75 MHz, (CD₃)₂SO, 25 °C, TMS): δ=175.0 (CO), 174.5 (CO), 151.6 (C), 129.8 (CH), 57.7 (CH₂), 56.2 (C), 54.0 (C), 26.2 (CH₂), 25.8 (CH₂), 15.74 (CH₂), 15.67 (CH₂).



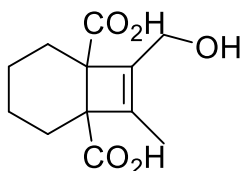
(6b) 7-(2-hydroxyethyl)bicyclo[4.2.0]oct-7-ene-1,6-dicarboxylic acid – Observed but not isolated

¹H NMR (400 MHz, (CD₃)₂SO, 25°C, TMS): δ=12.1 (b, 2H, 2x OH), 5.93 (t, *J*=1.7 Hz, 1H, CH), 4.54 (b, 1H, OH), 3.56 (t, *J*=7.2 Hz, 2H, CH₂), 2.27-2.11 (m, 2H, CH₂), 2.03-1.89 (m, 2H, CH₂), 1.74-1.59 (m, 2H, CH₂), 1.57-1.36 (m, 4H, 2x CH₂).



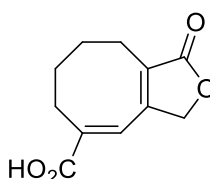
(6c) 6-(hydroxymethyl)bicyclo[3.2.0]hept-6-ene-1,5-dicarboxylic acid – Observed but not isolated

¹H NMR (400 MHz, (CD₃)₂SO, 25°C, TMS): δ=12.19 (b, 2H, 2x OH), 5.81 (t, *J*=1.9 Hz, 1H, CH), 4.82 (b, 1H, OH), 3.96 (dd, *J*=15.7, 24.5 Hz, 1H, CH₂), 1.82-1.64 (m, 4H, 2x CH₂), 1.61-1.53 (m, 2H, CH₂).



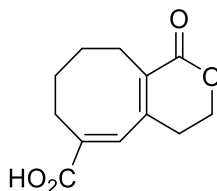
(6d) 7-(hydroxymethyl)-8-methylbicyclo[4.2.0]oct-7-ene-1,6-dicarboxylic acid

^1H NMR (400 MHz, $(\text{CD}_3)_2\text{SO}$, 25°C , TMS): δ =4.09-3.91 (m, 2H, CH_2), 1.99-1.83 (m, 2H, CH_2), 1.74-1.59 (m, 5H, $\text{CH}_3 + \text{CH}_2$), 1.55-1.42 (m, 3H, $\text{CH}_2 + \text{CH}_{2\text{A}}$), 1.40-1.29 (m, 1H, $\text{CH}_{2\text{B}}$); ^{13}C NMR (100 MHz, $(\text{CD}_3)_2\text{SO}$, 25°C , TMS): δ =175.4 (CO), 175.1 (CO), 142.2 (C), 139.8 (C), 56.4 (CH_2), 55.7 (C), 55.2 (C), 25.3 (CH_2), 24.5 (CH_2), 15.84 (CH_2), 15.83 (CH_2), 11.5 (CH_3); HRMS (ESI) m/z $[\text{M}+\text{Na}]^+$ calcd for $\text{C}_{12}\text{H}_{16}\text{NaO}_5$: 263.0890, found: 263.0893; IR (ATR): ν/cm^{-1} 1708 (s, C=O), 1689 (s, C=O), 1637 (m, C=C).



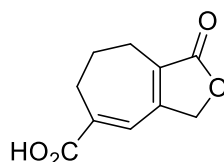
(7a) (*E*)-1-oxo-1,3,6,7,8,9-hexahydrocycloocta[c]furan-5-carboxylic acid^[4]

^1H NMR (400 MHz, $(\text{CD}_3)_2\text{CO}$, 25°C , TMS): δ =11.09 (b, 1H, OH), 7.27 (s, 1H, CH), 4.79 (td, J =2.6, 0.9 Hz, 2H, CH_2), 2.67-2.62 (m, 2H, CH_2), 2.45-2.40 (m, 2H, CH_2), 1.87-1.79 (m, 2H, CH_2), 1.73-1.65 (m, 2H, CH_2); ^{13}C NMR (100 MHz, $(\text{CD}_3)_2\text{SO}$, 25°C , TMS): δ =174.1 (CO), 152.1 (CO), 152.1 (C), 137.6 (C), 129.0 (CH), 128.6 (C), 71.0 (CH_2), 25.7 (CH_2), 25.0 (CH_2), 24.8 (CH_2), 20.4 (CH_2).



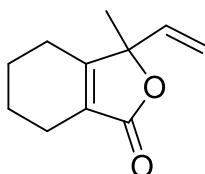
(7b) (*E*)-1-oxo-3,4,7,8,9,10-hexahydro-1H-cycloocta[c]pyran-6-carboxylic acid

^1H NMR (400 MHz, CD_3CN , 25°C , TMS): δ =7.14 (s, 1H, CH), 4.34 (t, J =6.2 Hz, 2H, CH_2), 2.47 (t, J =6.2 Hz, 2H, CH_2), 2.42-2.00 (br m, 4H, 2x CH_2), 1.59-1.35 (br m, 4H, 2x CH_2); ^{13}C NMR (100 MHz, CD_3CN , 25°C , TMS): δ =168.4 (CO), 166.3 (CO), 147.5 (C), 136.6 (C), 136.4 (CH), 128.8 (C), 66.9 (CH_2), 28.4 (CH_2), 28.1 (CH_2), 27.7 (CH_2), 24.3 (CH_2), 23.4 (CH_2); HRMS (ESI) m/z $[\text{M}+\text{H}]^+$ calcd for $\text{C}_{12}\text{H}_{15}\text{O}_4$: 223.0965, found: 223.0959.



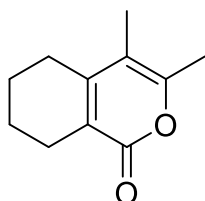
(7c) 1-oxo-3,6,7,8-tetrahydro-1*H*-cyclohepta[*c*]furan-5-carboxylic acid

^1H NMR (400 MHz, CD_3CN , 25°C , TMS): δ =7.06 (s, 1H, CH), 4.77 (t, J =2.9 Hz, 2H, CH_2), 2.78-2.73 (m, 2H, CH_2), 2.56-2.50 (m, 2H, CH_2), 1.91-1.85 (m, 2H, CH_2); ^{13}C NMR (100 MHz, $(\text{CD}_3)_2\text{SO}$, 25°C , TMS): δ =173.9 (CO), 168.0 (CO), 142.5 (C), 130.7 (C), 125.7 (CH), 71.1 (CH_2), 29.2 (CH_2), 26.8 (CH_2), 21.5 (CH_2); HRMS (ESI) m/z $[\text{M}+\text{H}]^+$ calcd for $\text{C}_{10}\text{H}_{11}\text{O}_4$: 195.0652, found: 195.0660.



(8) 3-methyl-3-vinyl-4,5,6,7-tetrahydroisobenzofuran-1(3*H*)-one

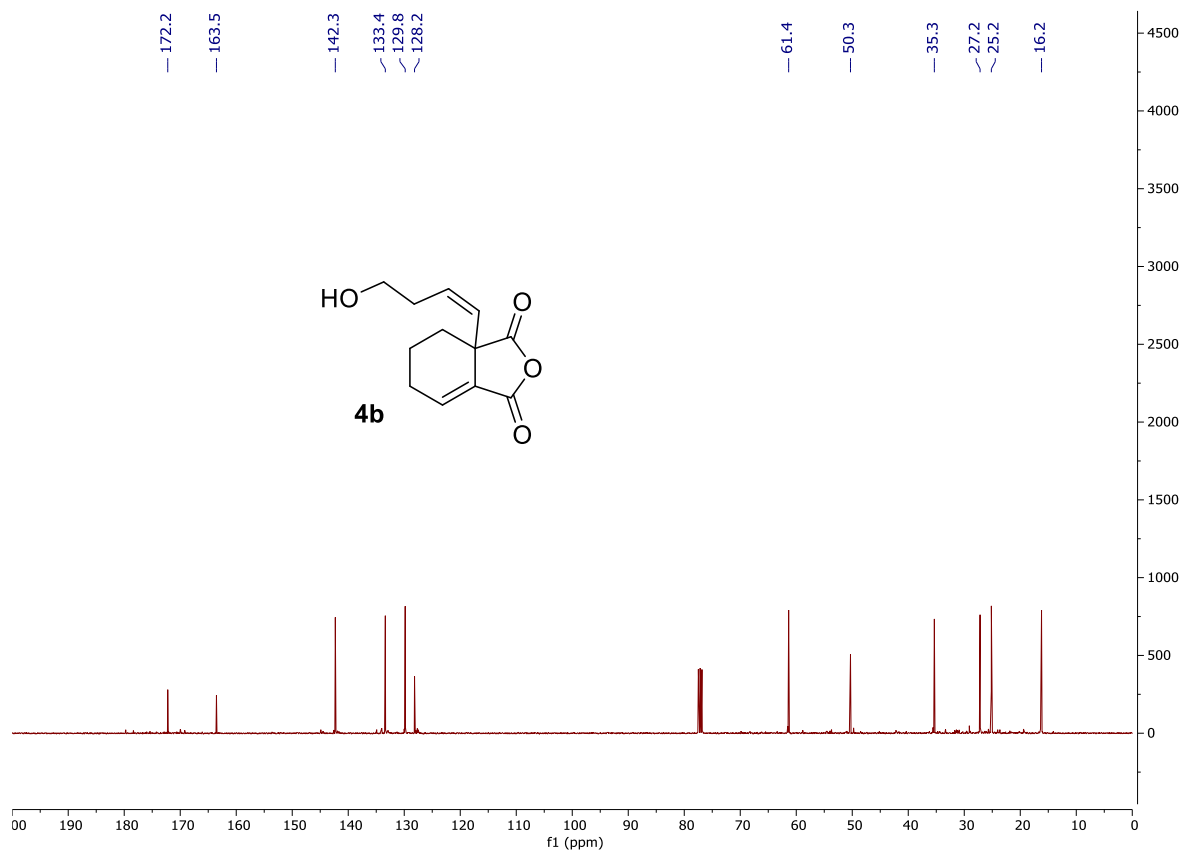
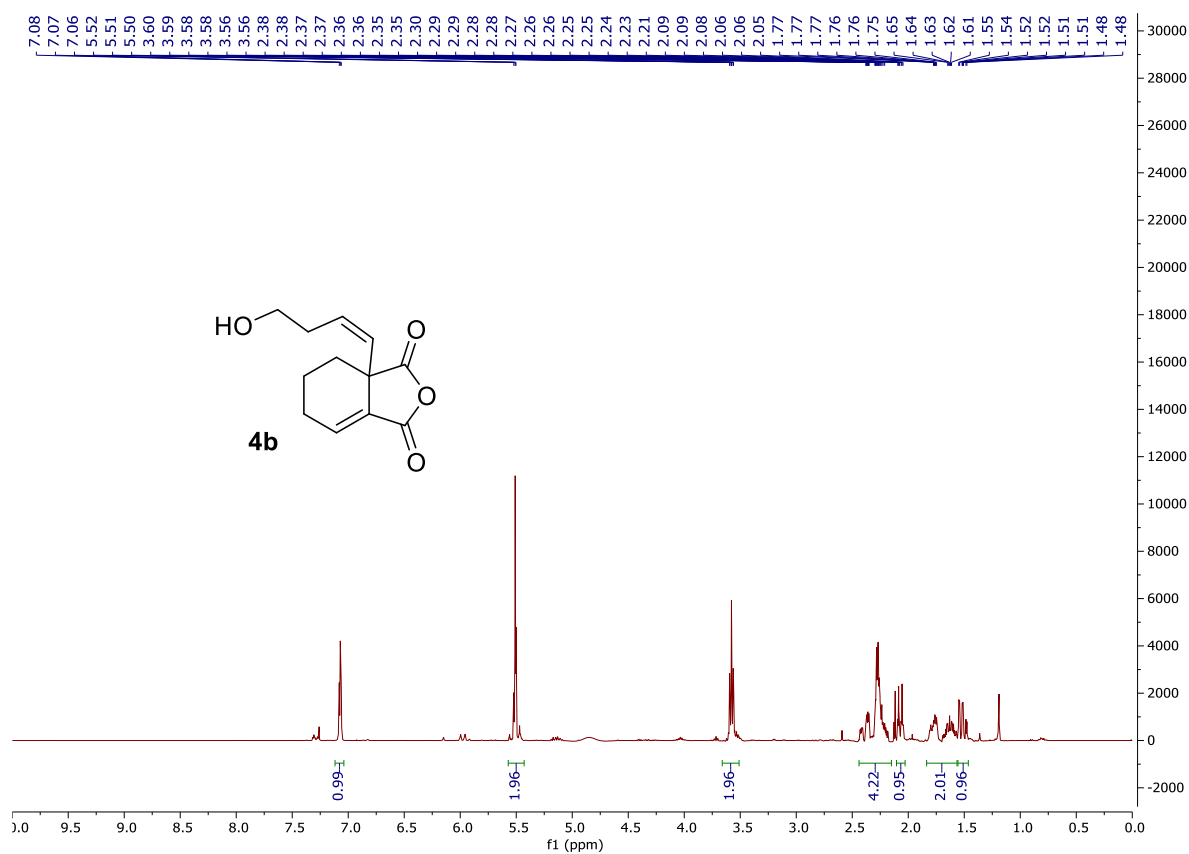
^1H NMR (400 MHz, CDCl_3 , 25°C , TMS): δ =5.75 (dd, J =17.3 Hz, 10.7 Hz, 1H; CH), 5.34 (d, J =17.3, 1H, $\text{CH}_{2\text{A}}$), 5.21 (d, J =10.7, 1H, $\text{CH}_{2\text{B}}$), 2.24-2.14 (m, 4H, 2x CH_2), 1.77-1.65 (m, 4H, 2x CH_2), 1.50 (s, 3H, CH_3); ^{13}C NMR (100 MHz, CDCl_3 , 25°C , TMS): δ =173.0 (CO), 166.6 (C), 137.1 (CH), 125.4 (C), 116.2 (CH_2), 87.3 (C), 22.2 (CH_3), 22.1 (CH_2), 21.8 (CH_2), 21.7 (CH_2), 20.0 (CH_2); HRMS (ESI) m/z $[\text{M}+\text{H}]^+$ calcd for $\text{C}_{11}\text{H}_{15}\text{O}_2$: 179.1067, found: 179.1024; IR (ATR): ν/cm^{-1} 1748 (s, C=O), 1678 (m, C=C), 1641 (m, C=C).



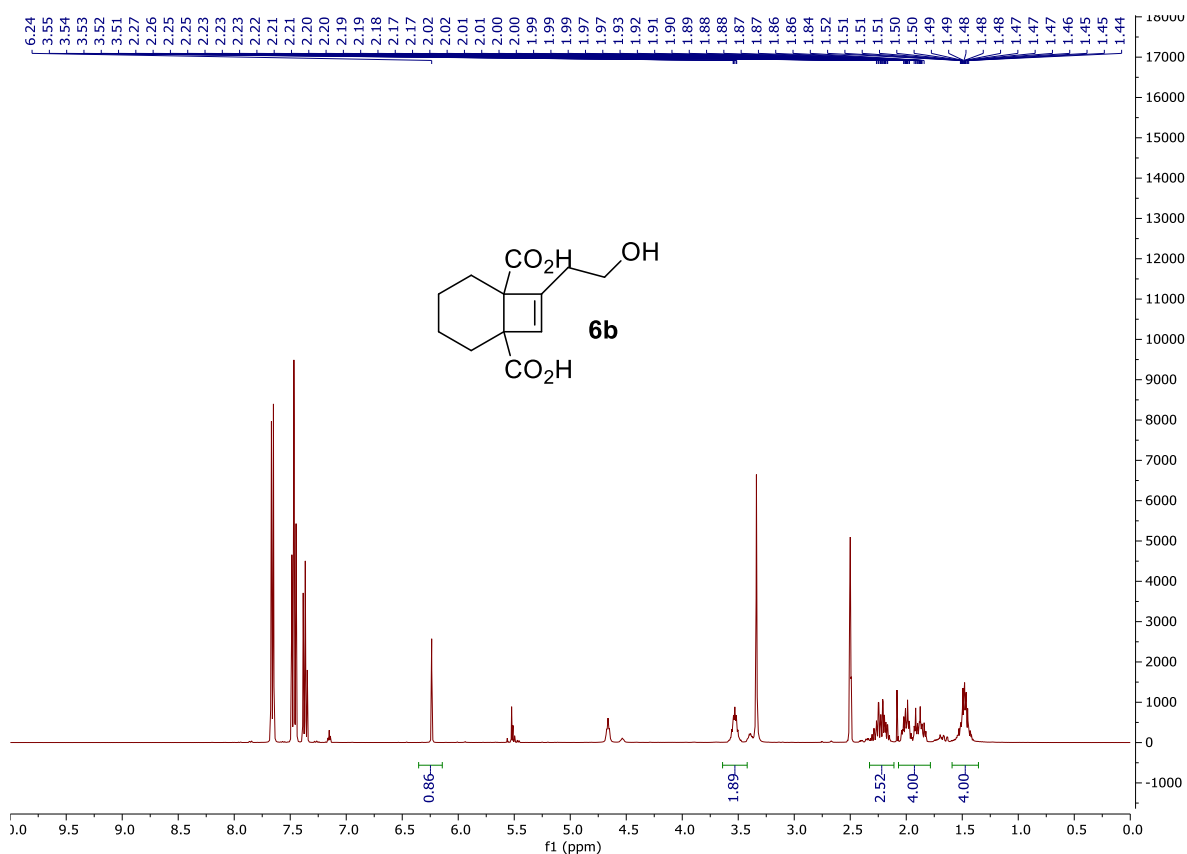
(9) 3,4-dimethyl-5,6,7,8-tetrahydro-1*H*-isochromen-1-one

^1H NMR (400 MHz, CDCl_3 , 25°C , TMS): δ =2.47-2.35 (m, 4H, 2x CH_2), 2.19 (s, 3H, CH_3), 1.87 (s, 3H, CH_3), 1.76-1.63 (m, 4H, 2x CH_2); ^{13}C NMR (100 MHz, CDCl_3 , 25°C , TMS): δ =163.8 (CO), 153.1 (C), 152.3 (C), 120.2 (C), 111.3 (C), 27.2 (CH_2), 23.6 (CH_2), 21.9 (CH_2), 21.5 (CH_2), 17.4 (CH_3), 12.1 (CH_3); HRMS (ESI) m/z $[\text{M}+\text{Na}]^+$ calcd for $\text{C}_{11}\text{H}_{14}\text{NaO}_2$: 201.0886, found: 201.0894; IR (ATR): ν/cm^{-1} 1695 (s, C=O), 1643 (s, C=C), 1565 (s, C=C).

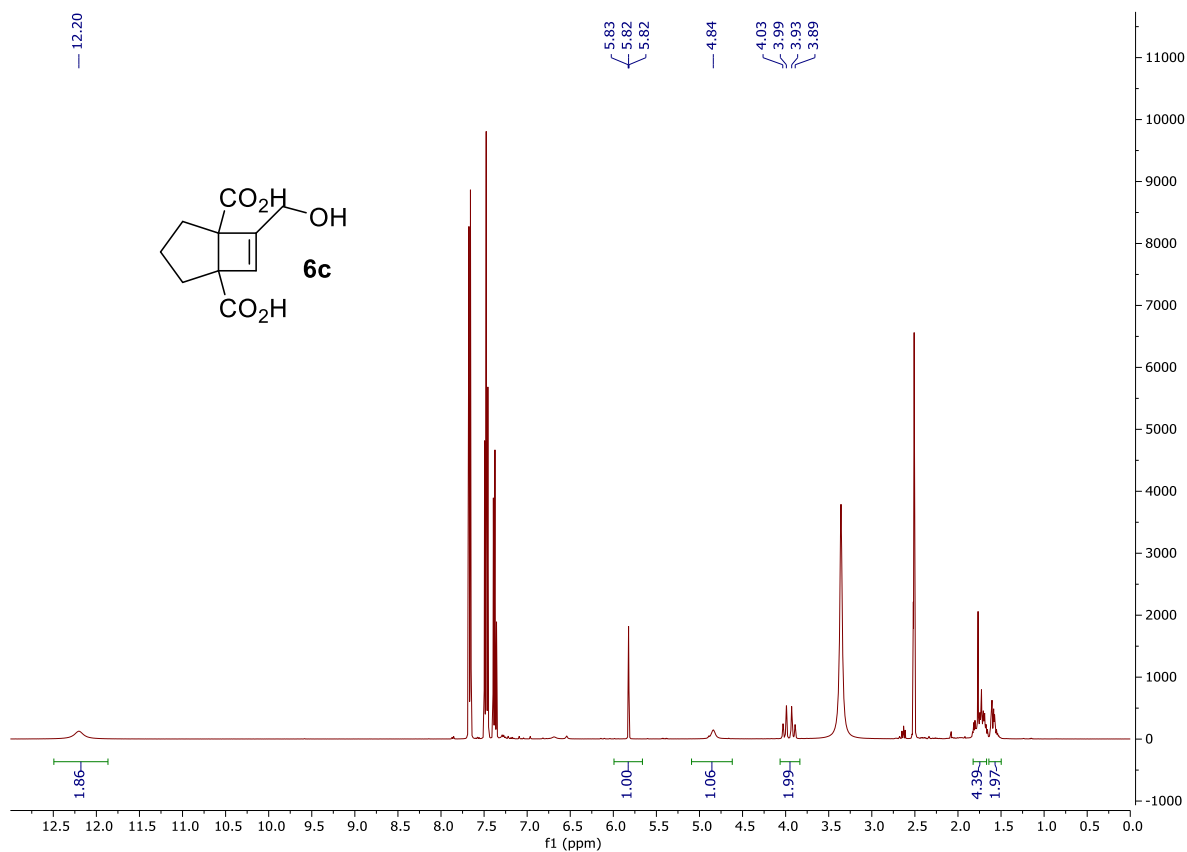
8. NMR Spectra

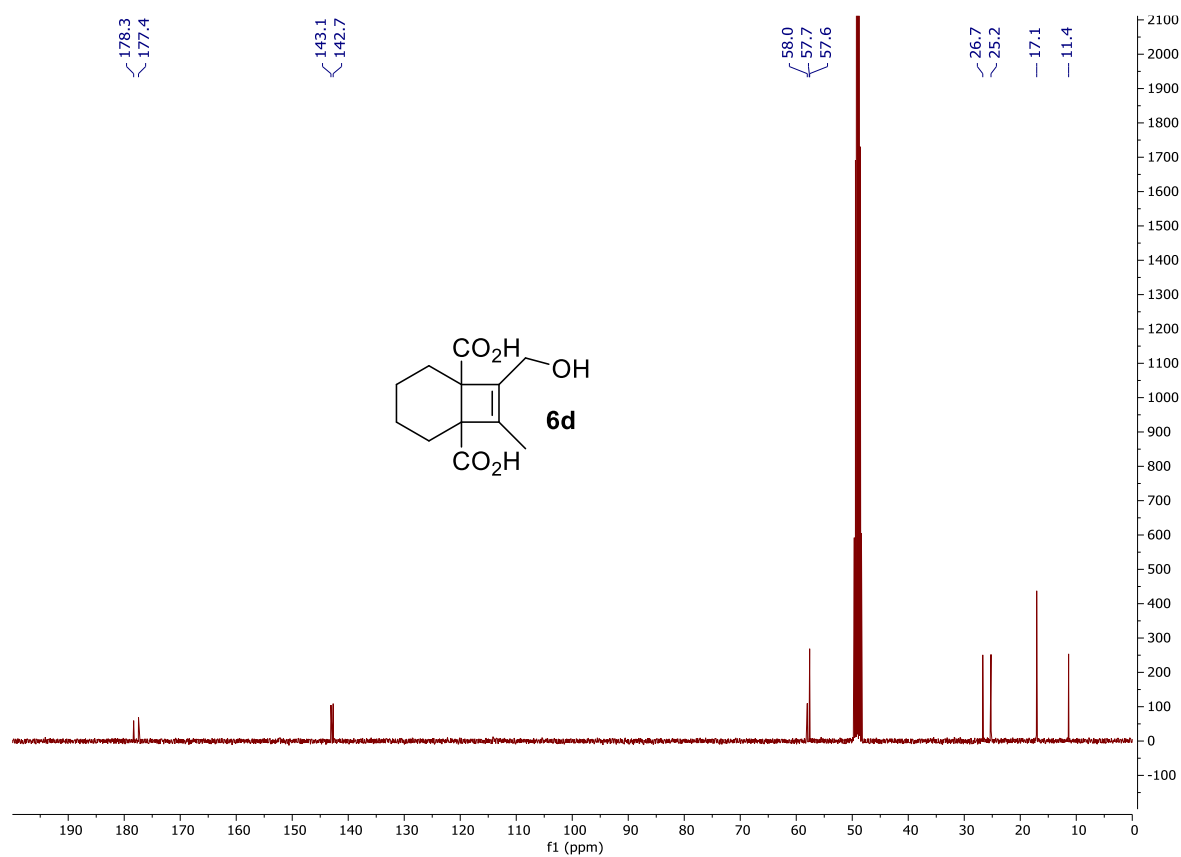
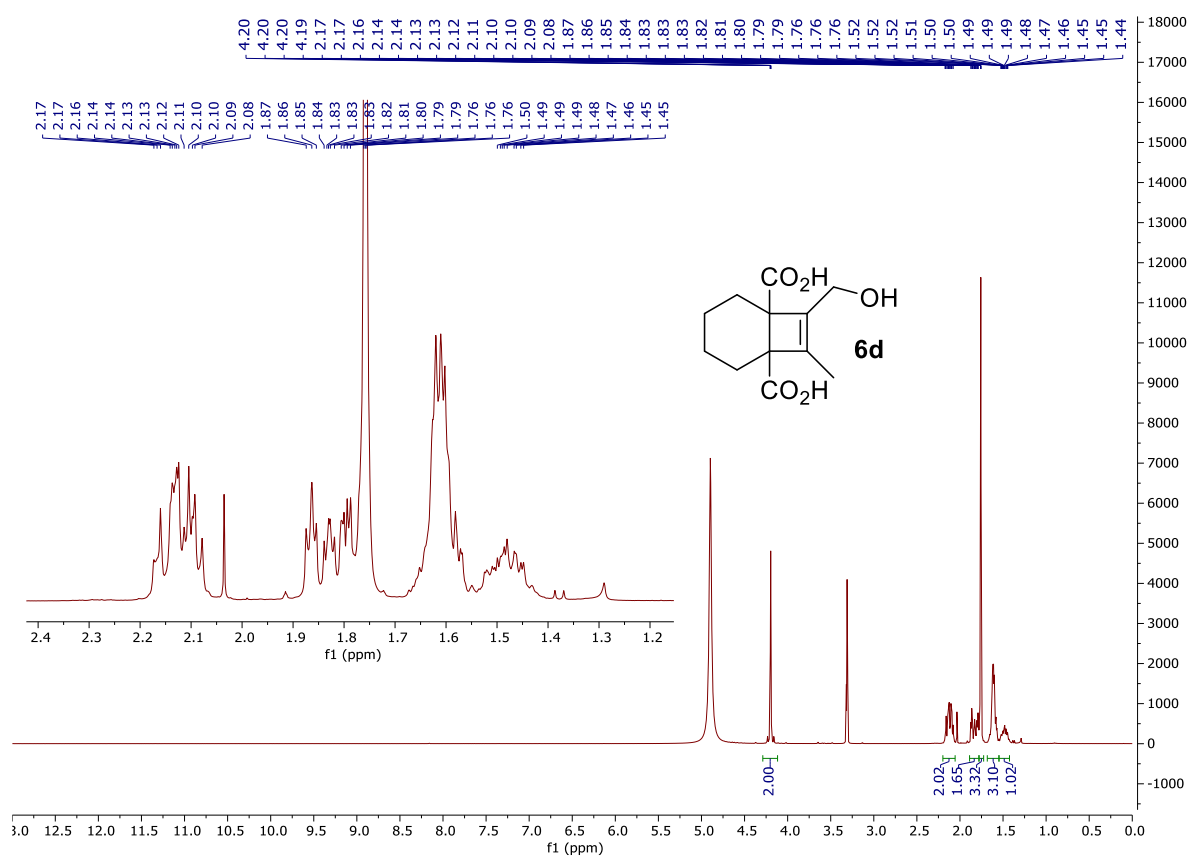


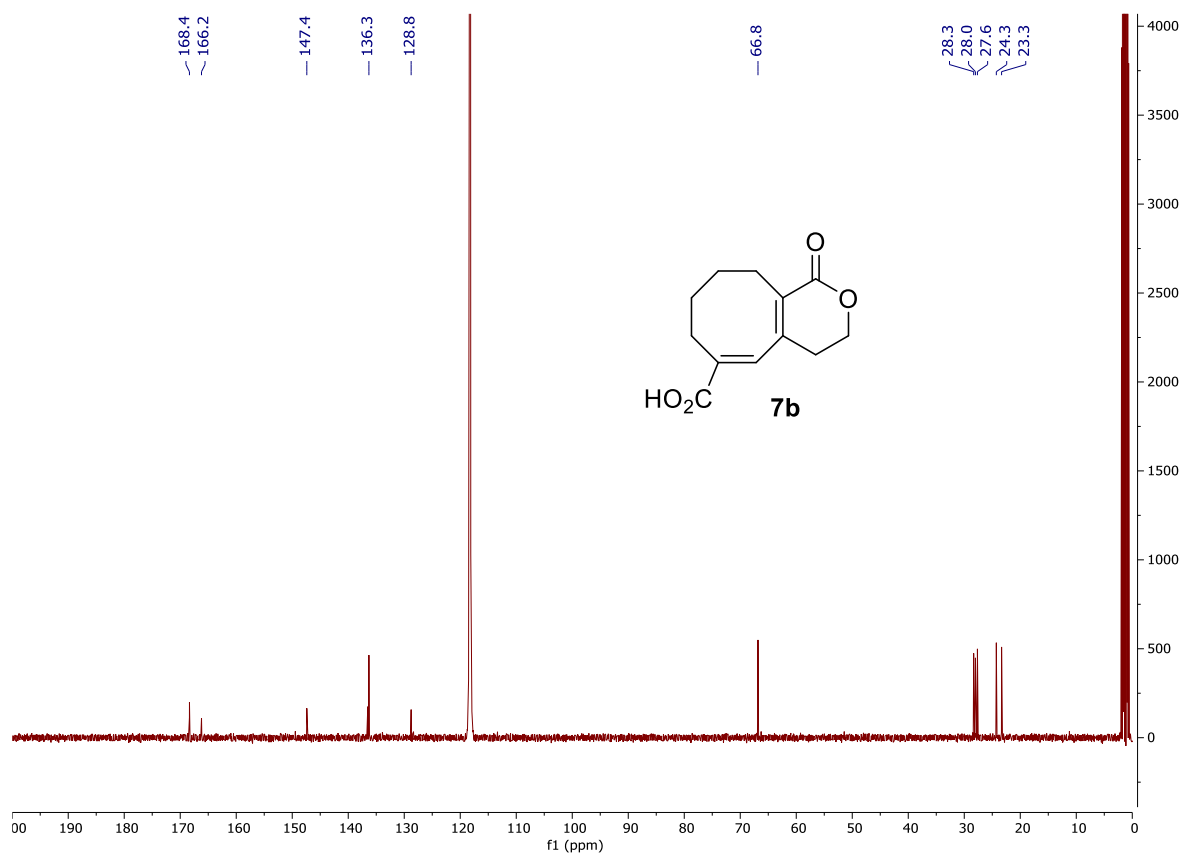
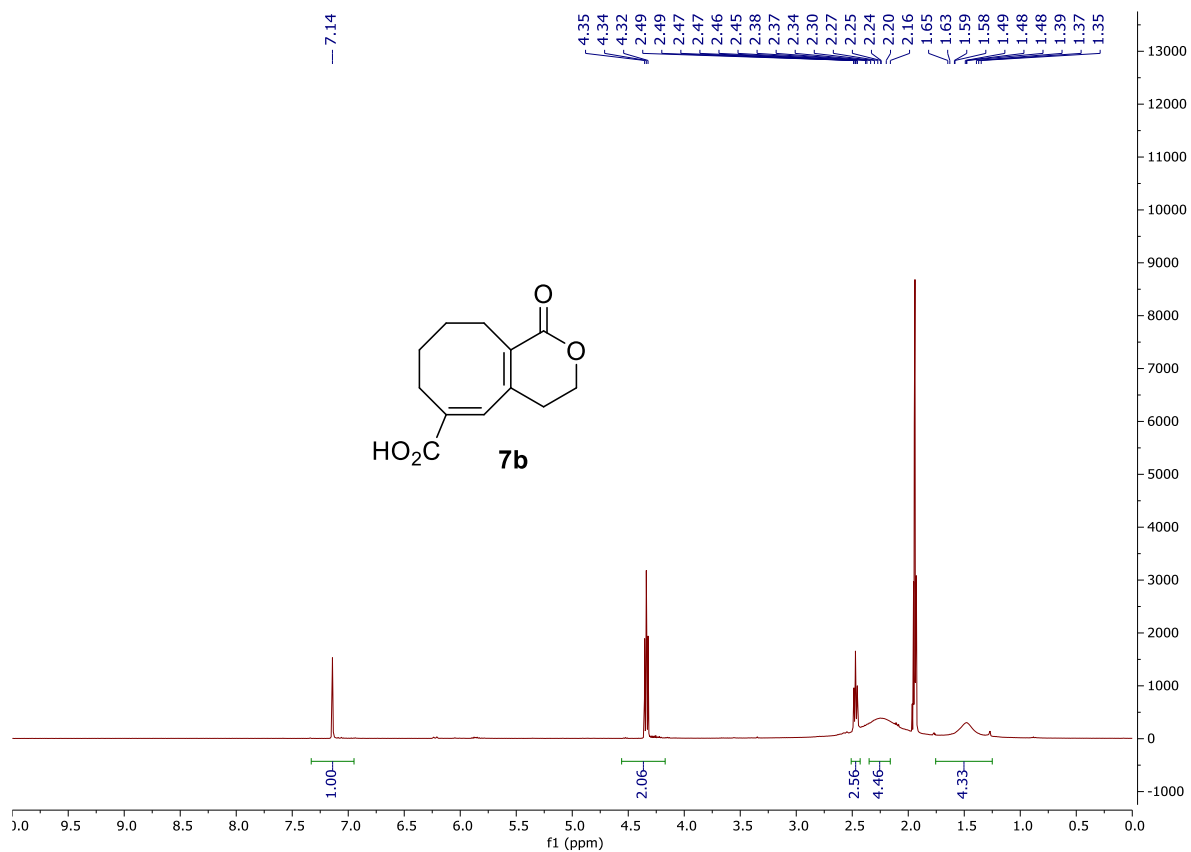
6b – Observed in the presence of biphenyl (7.3 – 7.8 ppm) but not isolated

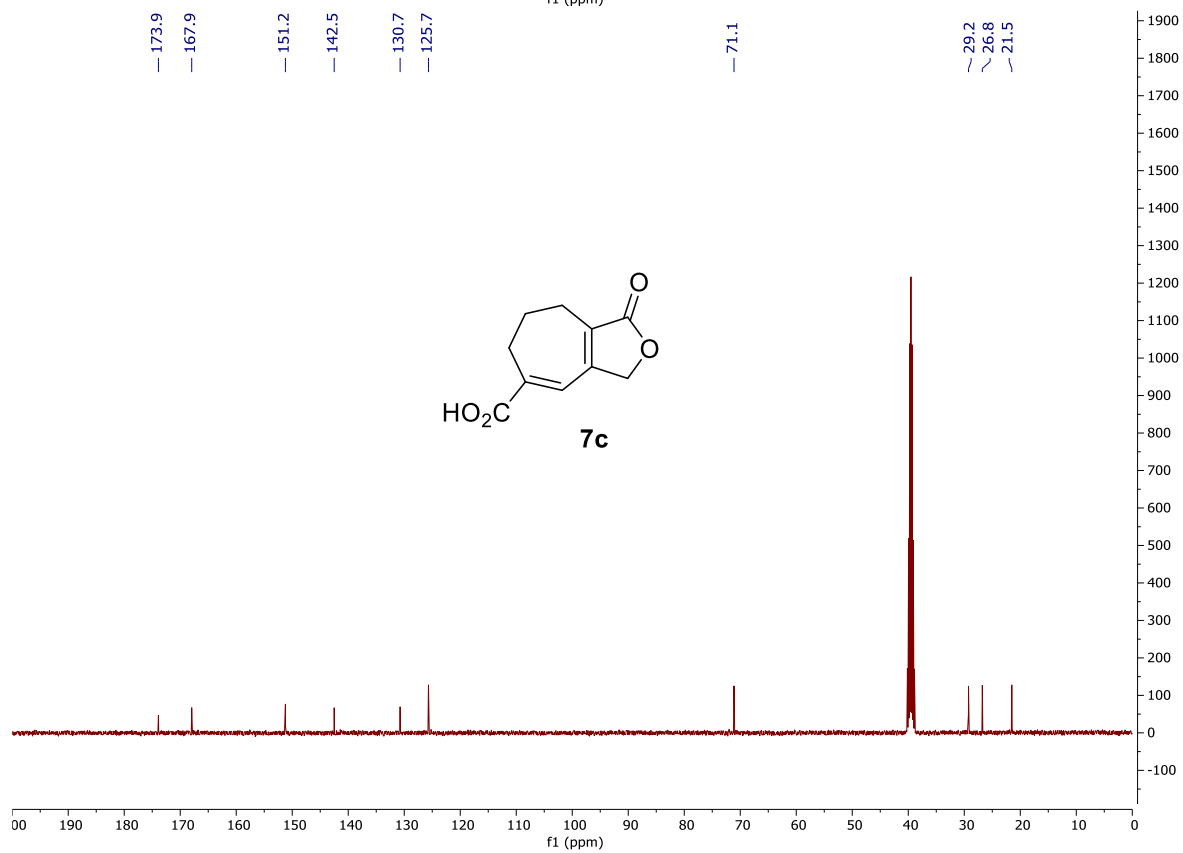
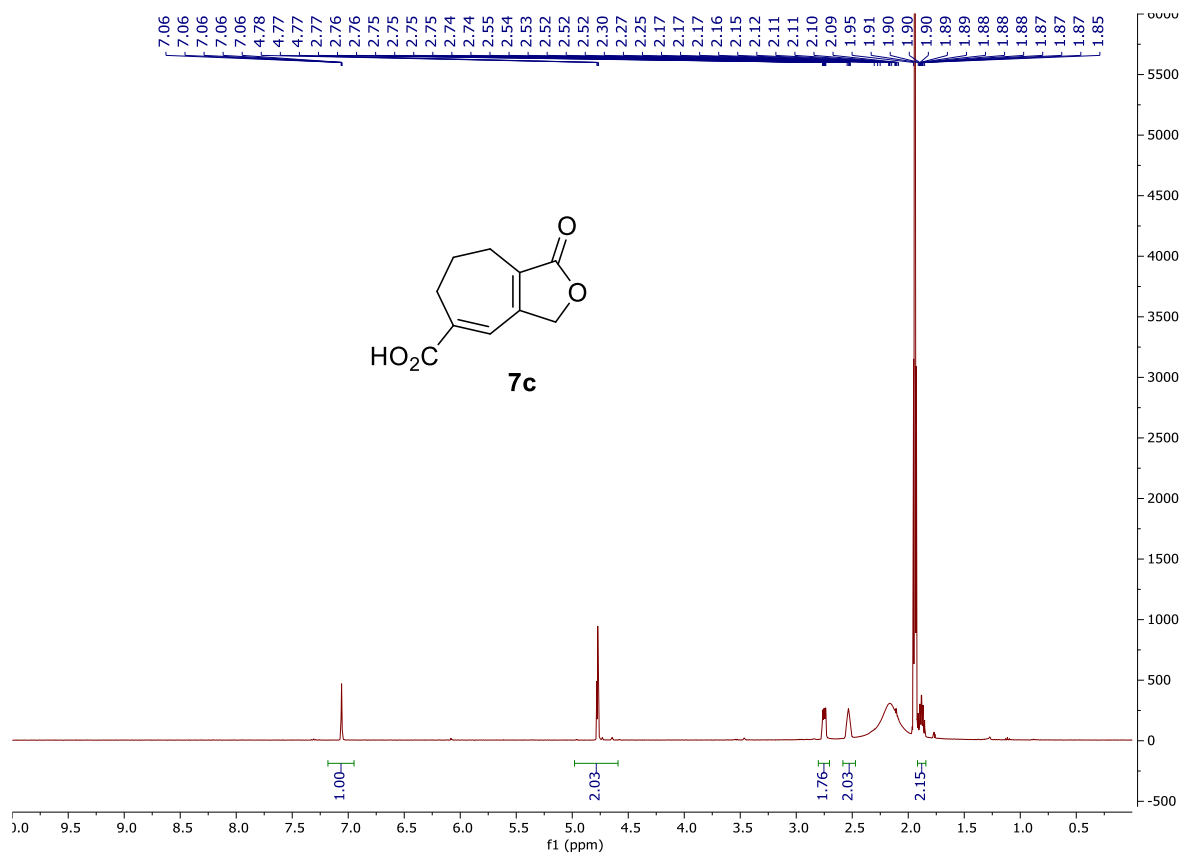


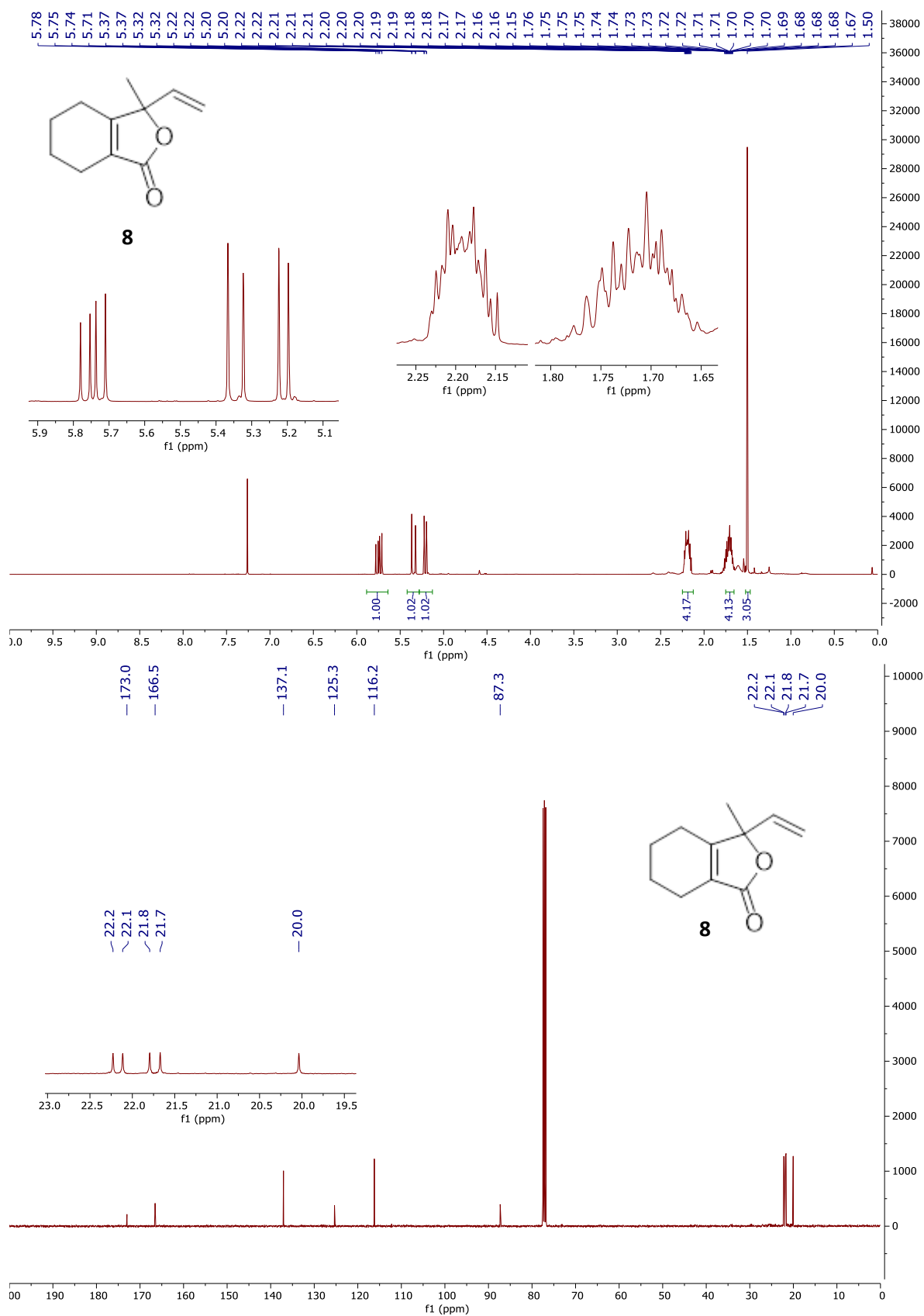
6c - Observed in the presence of biphenyl (7.3 – 7.8 ppm) but not isolated

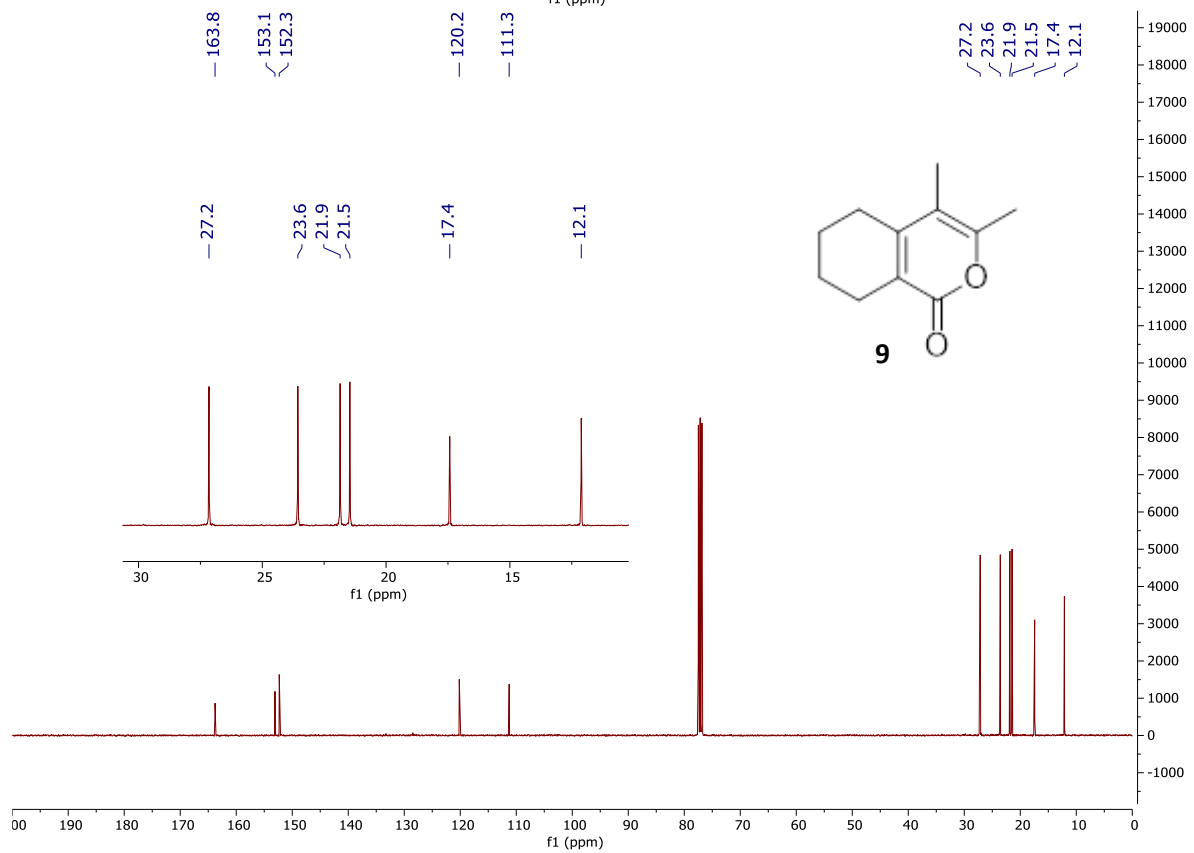
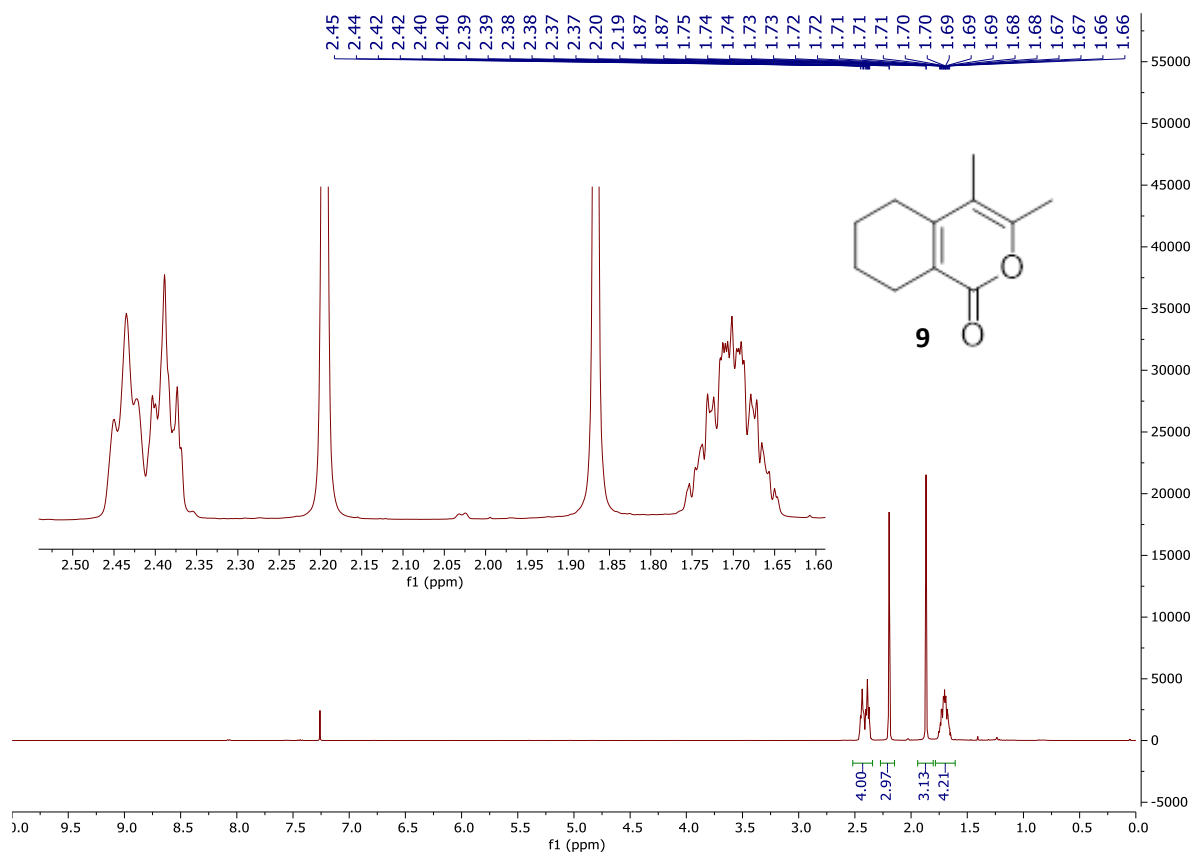












9. Time Resolved Infrared Spectroscopy (TRIR)

9.1. Description of Time Resolved Infrared Spectroscopy (TRIR) setup

The TRIR spectroscopy apparatus at the Nottingham has been described previously.^[7] Briefly, fundamental pulses (800 nm, 100 fs, 80 MHz) are generated with a commercial Ti:Sapphire oscillator (Spectra-Physics MaiTai) and fundamental pulses are amplified in a Ti:Sapphire amplifier (Spectra-Physics SpitfirePro) to produce 800 nm, 100 fs, 1 kHz, 2 mJ pulses. Half of the output is used to pump a TOPAS-C (Light Conversion) to produce tunable IR pulses using a difference frequency generator and the other part of the output is used to pump a harmonic generator (Time Plate Tripler, Minioptic Technology) to produce either 400 nm and 266 nm 100 fs pulses. The 400/266 nm pulses are used as pump beam and are focused onto the sample and delayed up to 2 ns with respect to the IR pulses by a translational stage (LMA Actuator, Aerotech). Part of the IR pulse is reflected onto a single-element mercury cadmium telluride (MCT) detector (Kolmar Technology) to serve as a reference, and the rest of the output is used as the probe and is focused and overlaps with the pump beam at the sample position. The polarization of the pump pulse was set at the magic angle (54.7°) relative to the probe pulse to avoid rotational diffusion. The broad-band transmitted probe pulse is detected with an 128 element MCT array detector (Infrared Associates). The array detector is mounted in the focal plane of a 250 mm IR spectrograph (DK240, Spectra Product) with a 150 grooves/mm grating. For TRIR measurements on timescales > 0.5 ns, a Q-switched Nd : YVO laser (ACE- 25QSPXHP/MOPA, Advanced Optical Technology, UK) was employed as a pump source which is synchronized to the Spitfire Pro amplifier.

9.2. Time Resolved Infrared Data

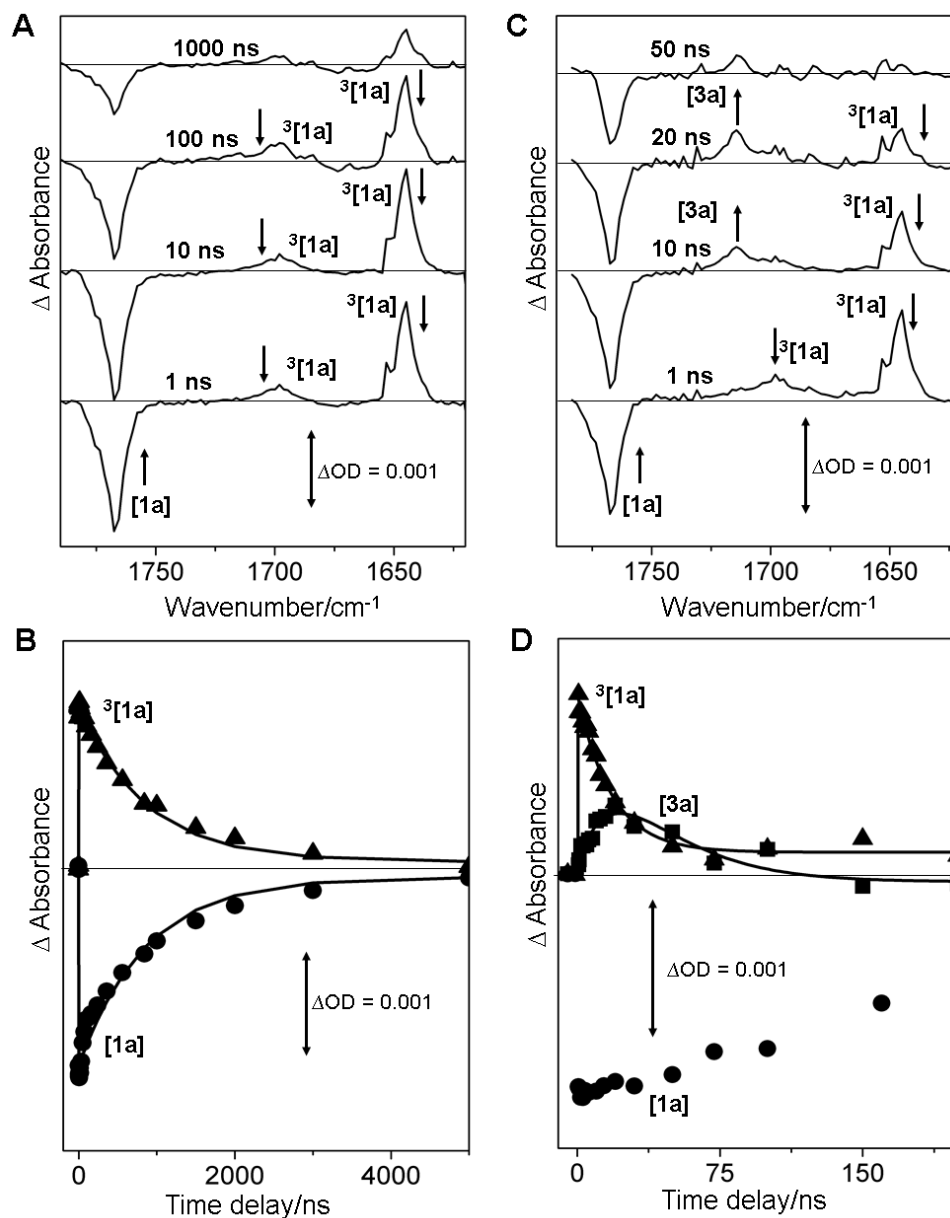


Figure S9. (A) ns TRIR spectra of **1a** (11 mM) in CD₃CN at selected pump-probe time delays. The bands at 1645 cm⁻¹, 1700 cm⁻¹ is assigned to the ³ππ* state of **1a**. (B) TRIR decay traces obtained from the ns experiment as shown in A. The decay of ³[**1a**] (1645 cm⁻¹ peak intensity kinetics) state and bleach recovery (1774 cm⁻¹ peak intensity kinetics) are with lifetime of 1.05 (± 0.05) μs (C) ns TRIR spectra of mixture of **1a** (11 mM) and **2a** (120 mM) at selected pump-probe time delays. (D) TRIR decay traces obtained from the ns experiment as shown in C, showing the quenching of the ³[**1a**], formation and decay of bi-radical intermediate **3a** and partial bleach recovery of **1a**. The decay of ³[**1a**] state is associated with the formation of **3a** with time constant of 20(±2) ns.

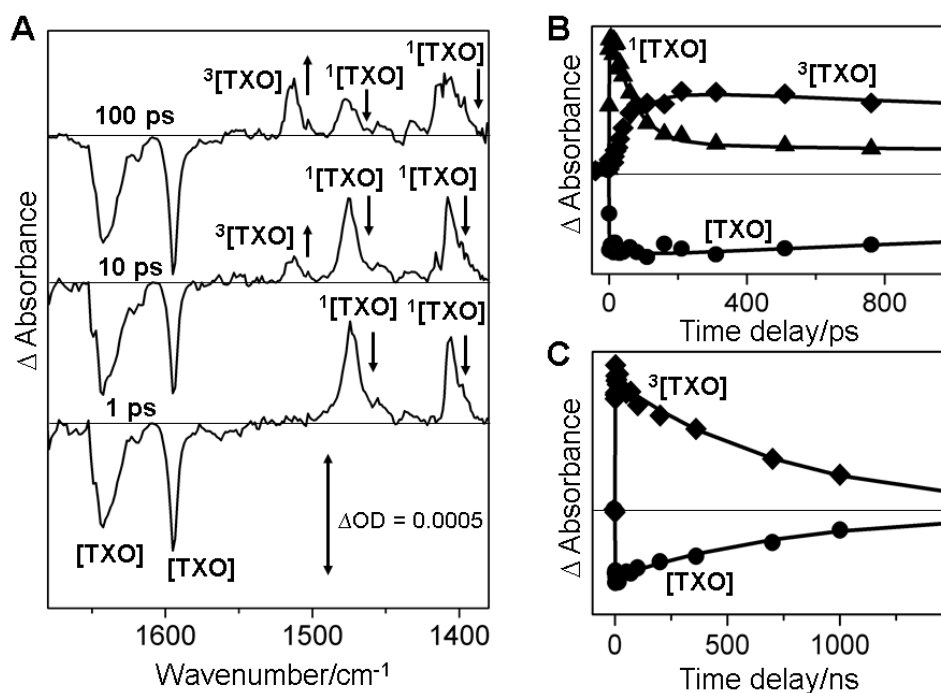


Figure S10. (A) ps TRIR spectra of TXO at selected pump-probe time delays in CD_3CN after 355 nm photoexcitation. (B) ps TRIR kinetic traces showing decay of $^1[\text{TXO}]$ state, formation of $^3[\text{TXO}]$ state and partial bleach recovery of ground state. The singlet state decays with the lifetime of $60(\pm 4)$ ps. The decay of excited singlet state is associated with the formation of $^3[\text{TXO}]$ state. (C) ns TRIR kinetic traces showing decay of $^3[\text{TXO}]$ state and bleach recovery kinetics. The lifetime of the triplet state is $760(\pm 30)$ ns.

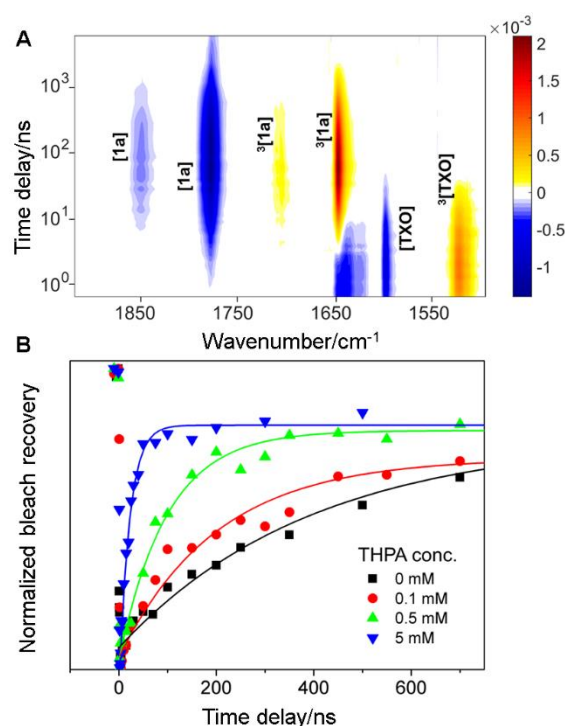


Figure S11. (A) 2D contour map of the TRIR spectra of the mixture of TXO (1.2 mM) + **1a** (12 mM) in CD_3CN solution after 355 nm photoexcitation. (B) Bleach recovery kinetics of $[\text{TXO}]$ with the indicated concentration of **1a** (THPA). The obtained bimolecular rate constant is $k_q = 6.7 \times 10^9 \text{ M}^{-1}\text{s}^{-1}$.

9.3. Characterization of the transient species:

The photoexcitation of TXO (at 355 nm) in presence of **1a** (THPA) and propargyl alcohol generates $^3[\text{TXO}]$, $^3[\text{1a}]$, **3a** and the final products **5a (major)** and **4a (minor)**. The TRIR studies include complete excited state characterization of **TXO**, **1a** by direct photoexcitation followed by quenching studies of the **TXO+1a** and **TXO+1a+propargyl alcohol** reaction mixtures. Our initial studies confirm that PAOH alone has little effect on the excited triplet state lifetime of TXO.

The ns TRIR spectra at selected time delays after 355 nm photoexcitation (TXO is excited exclusively) of TXO (1.2 mM)+**1a** (12 mM) in CD₃CN are presented in **Figure S10**. In the ns timescale, both the $^3[\text{TXO}]$ and $^3[\text{1a}]$ contribute to the TRIR signal. The assignment of the vibrational modes to the individual species is done by performing TRIR studies on TXO and **1a** separately (Figure **S10** and Figure **S9** respectively). Because the ns TRIR spectra of **1a** ($\lambda_{\text{exc}} = 266$ nm) alone show bleaches at 1774 cm⁻¹ and triplet excited state bands at 1700, 1645 cm⁻¹ (Figure **S9**), we assigned these bands safely to the ground state **1a** and $^3[\text{1a}]$ respectively. Bleaches at 1637 and 1594 cm⁻¹ are due to the **TXO** and the 1518cm⁻¹ band is assigned to the $^3[\text{TXO}]$ based on the TRIR experiments on TXO alone (Figure **S10**)The formation of $^3[\text{1a}]$ following the 355 nm excitation confirms the triplet-triplet energy transfer process.

9.4. Kinetic rate constants for the sensitized reaction:

The ns TRIR studies on the **TXO+1a** mixture after 355 nm photoexcitation allows us to isolate the reaction kinetics for the generation of $^3[\text{1a}]$ and its return to the ground state. We performed a global kinetic analysis to obtain quantitative information on the kinetics. From the above discussion, it follows that at least three kinetic components – $^3[\text{TXO}]$, $^3[\text{1a}]$, and infinite component are required to completely describe the ns TRIR data. Indeed, three kinetic components describe the data in a satisfactory manner. The resulting time constants are $\tau_1 = 12.9 (\pm 2)$ ns and $\tau_2 = 536 (\pm 25)$ ns and a long-lived component. The τ_1 is the lifetime of $^3[\text{TXO}]$ state, and τ_2 is the lifetime of $^3[\text{1a}]$ state. The triplet energy transfer from the excited **TXO** to the ground state of **1a** leads to a strongly reduced $^3[\text{TXO}]$ state lifetime (in absence of THPAA the $^3[\text{TXO}]$ lifetime is 760 (± 30) ns). The triplet energy transfer rate k_T is obtained by the following equation:

$$k_T = \frac{1}{\tau} - \frac{1}{\tau_0} = 7.7 \times 10^7 \text{ s}^{-1} \dots\dots\dots (\text{S1})$$

where τ is the triplet lifetime in the presence of quencher and τ_0 is triplet lifetime in the absence of quencher. For bimolecular quenching experiments, in the low concentration limit of the quencher (dynamic quenching), the kinetics is often pseudo-first order. The plot of the quenching rate constants

(Figure S11(B)) versus **1a** concentrations confirms a linear relationship indicating that in this concentration regime the quenching is controlled by diffusion.

Next, we explored the kinetics of the [2+2] photocycloaddition reaction by studying the kinetics of the **TXO+1a+2a** solution. We have to consider many different chemical species for the kinetic analysis. Therefore, kinetics of the IR bands associated with the individual species are considered for the detailed kinetic analysis. Selected kinetic traces associated with the various species are presented in Figure S12. After excitation of TXO, the $^3[\text{TXO}]$ state (1518 cm^{-1} mode) decays with the time constant of $\tau_{\text{decay}} = 15(\pm 3)\text{ ns}$ with the bleach recovery (1594 cm^{-1}) with the time constant of $\tau_{\text{recovery}} = 14(\pm 2)\text{ ns}$. The decay of the $^3[\text{TXO}]$ state is associated with the formation of the $^3[\text{1a}]$ (1645 cm^{-1} , $\tau_{\text{rise}} = 12.5(\pm 2)\text{ ns}$). The bimolecular reaction between $^3\text{THPAA}$ with PAOH leads to the formation of bi-radical species (1715 cm^{-1}) with the time constant of $28(\pm 4)\text{ ns}$. The decay of the radical species with the time constant of $37.4(\pm 5)\text{ ns}$ leads to the formation of final product (1778 cm^{-1} mode)

Upon 266 nm excitation of **1a**, the singlet excited state ($^1[\text{1a}]$) rapidly decays to the ground state predominantly through ultrafast internal conversion. Beside ultrafast internal conversion, it yields $^3[\text{1a}]$ with triplet quantum yield of $\eta_{\text{ISC}} \approx 0.33$ (obtained from bleach recovery). From the direct TRIR measurements of **1a+2a** mixture, we conclude that the long-lived triplet state of **1a** involves in the [2+2] cycloaddition reaction, not the singlet excited state. The triplet-triplet energy transfer (TTET)

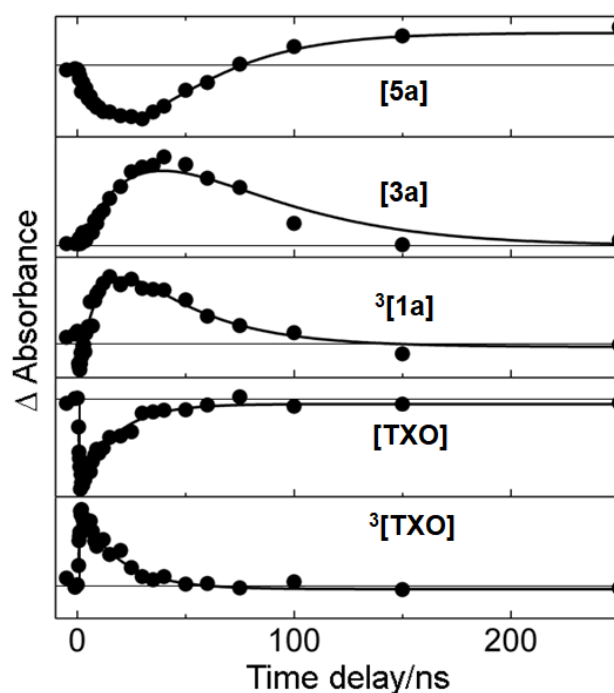


Figure S12. Peak position kinetics of IR modes associated with various species after photoexciting ($\lambda_{\text{exc}} = 355\text{ nm}$) a solution of **TXO** (1.2 mM)+**1a** (12 mM)+**2a** (120 mM) in CD_3CN .

quantum yield from $^3[1a]$ to the ground state **2a** (at a particular concentration) can be obtained by the following equation:

$$\phi_{TTET} = \frac{1/\tau}{1/\tau + 1/\tau_0} \dots\dots\dots (S2)$$

Where τ is the lifetime of $^3[1a]$ state in the presence of quencher **2a** and τ_0 is the lifetime $^3[1a]$ state in the absence of quencher. The complete quantum yield of the **3a** formation is therefore

$$\phi_{diradical-non\ sensitized} = \eta_{ISC,1a} \times \phi_{TTET(3[1a] \rightarrow 2a)} \dots\dots\dots (S3)$$

Our calculation yields $\phi_{diradical-non\ sensitized} \approx 0.32$ for the quantum yield of the formation of **3a** by direct photoexcitation. Using equation (2) we obtain the TTET from the $^3[TXO]$ to the ground state of **1a** and the energy transfer efficiency from $^3[1a]$ to **2a**. The total quantum yield formation of **3a bi-radical** for the sensitized reaction is given by

$$\phi_{bi-radical-sensitized} = \eta_{ISC,TXO} \times \phi_{TTET(3[TXO] \rightarrow [1a])} \times \phi_{TTET(3[1a] \rightarrow [2a])} \dots\dots (S4)$$

The triplet quantum yield of TXO ($\eta_{ISC,TXO}$) in ACN is 0.66. By applying equation (2) we can obtain $\phi_{TTET} (^3[TXO] \rightarrow [1a])$ and $\phi_{TTET} (^3[1a] \rightarrow [2a])$. Overall we found $\phi_{bi-radical-sensitized} \approx 0.61$ in CD_3CN . Similar kinetic analysis in CH_2Cl_2 solvent yields $\phi_{bi-radical-sensitized} \approx 0.53$.

10. Raman Monitoring

10.1. Photochemical step

Raman spectroscopic measurements of the photochemical step were performed using a Kaiser Optical Systems Inc. RXN2 spectrometer, equipped with a sapphire tipped MarqMetrix BallProbe®. The photolysis was performed in an immersion well reactor using a 125 W medium pressure mercury lamp from Photochemical Reactors LTD. The Raman probe was inserted within an external sampling loop which was fed with the circulating reaction mixture *via* peristaltic pumps, in order to avoid exposure of the spectrometer detector to the mercury lamp light. The Spectra were collected using an excitation wavelength of 785 nm with a 400 mW laser power and a detector exposure time of 30 s with 10 averaged scans. The spectra collected during the course of the reaction are displayed in Figure S13.

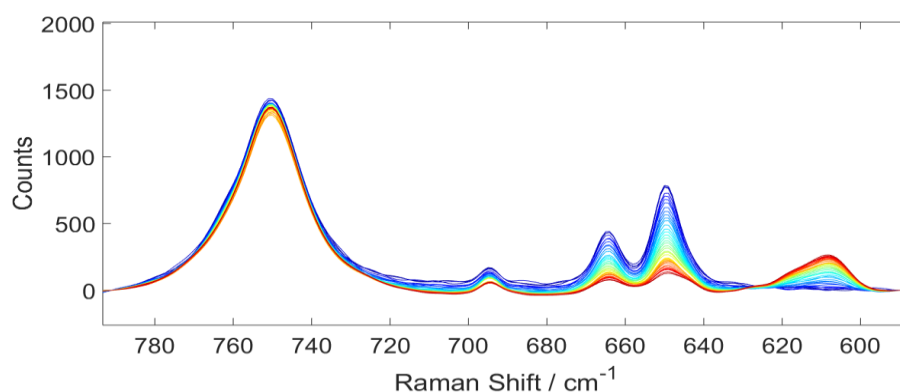


Figure S13 – Raman spectra of the photolysis with time (blue to red) in the ring and bridged skeleton region showing the depletion of the THPA at ca. 650 and at 665 cm⁻¹ and the growth of the bridged product peak at 607 cm⁻¹.

From these spectra the kinetics of the reaction could be monitored by tracking the normalised intensity of the THPA starting material vibration at 665 cm⁻¹ and the bridged product at 607 cm⁻¹ as a function of time (**Figure S14**).

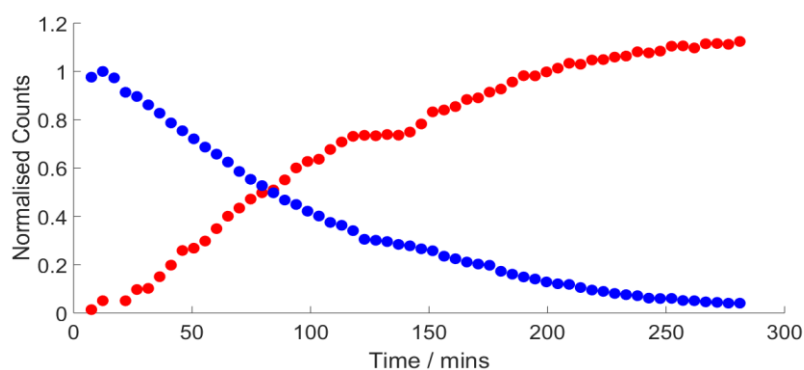


Figure S14 – Kinetics of the photochemical step obtained from the normalised intensity of the THPA starting material vibration at 665 cm⁻¹ (blue) and the bridged product at 607 cm⁻¹ (red).

During the course of the reaction the carbonyl region of the Raman spectrum also exhibited this behaviour with the disappearance of the THPA vibrations at *ca.* 1677, 1773 and 1845 cm^{-1} and the appearance of the bridged product peak at 1642 cm^{-1} . This is demonstrated in Figure S15.

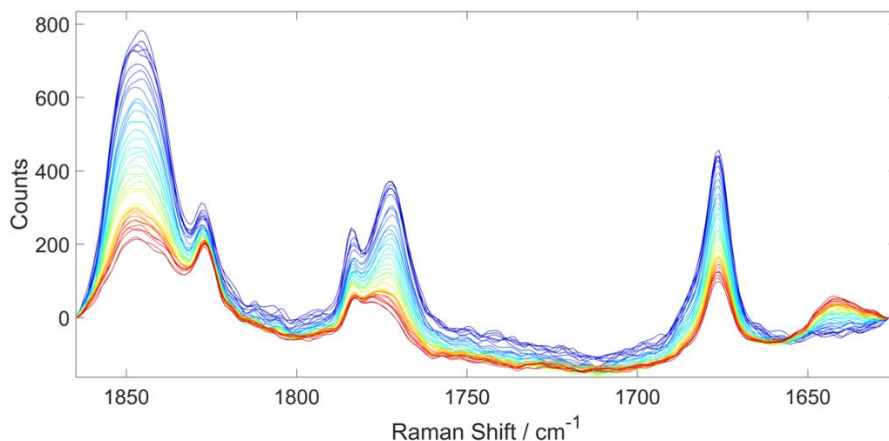


Figure S15 – Raman spectra of the photolysis with time (blue to red) in the carbonyl region showing the depletion of the THPA at *ca.* 1677, 1773 and 1845 cm^{-1} and the growth of the bridged product peak at 1642 cm^{-1} .

10.2. Thermal steps

Raman spectroscopic measurements of the thermal reaction was again achieved using a Kaiser Optical Systems Inc. RXN2 spectrometer, equipped with a sapphire tipped MarqMetrix BallProbe®. These spectra were collected with the same detector exposure and laser power (30 s, 10 scans and 400 mW power) as the photochemical step, however the sampling was obtained *via* the submerging of the probe in a sample collection vessel of the outlet of the thermal flow reactor. The thermal reaction was run at 225°C and 150 bar, at residence times ranging from 0.125 to 8 mins. Normalised Raman spectra of the product and starting material are shown in Figure S16.

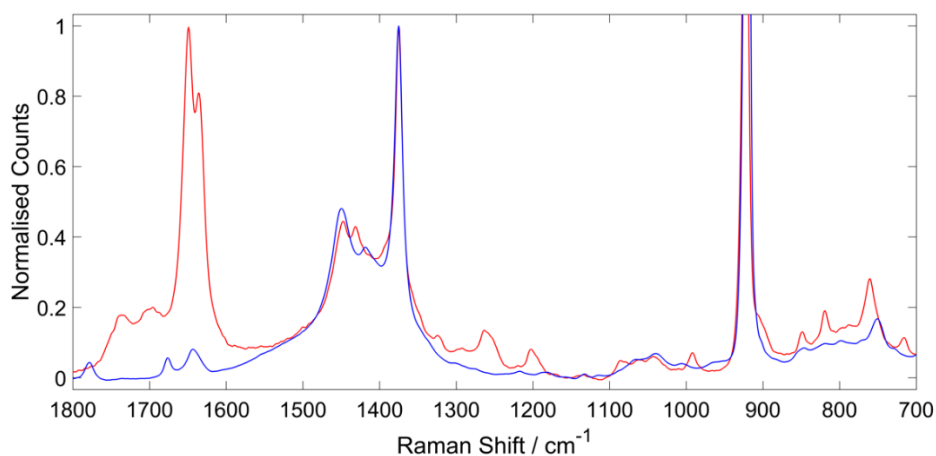


Figure S16 – Normalised Raman spectra of the both the starting material (blue) and product 7a (red) of the thermal step of the reaction.

The Spectra in Figure **S17** show the effect of the residence time on the yield of the product, as indicated by the height of the characteristic **7a** product modes. This is particularly evident for the 1650 cm^{-1} vibration. Using the height of this mode and plotting it as a function of residence time, it can be seen that the yield of the product increases as the residence time within the thermal reactor increases from 0.125 to 7 mins. However as this residence time increases past this to 8 mins, the yield starts to decrease due to the formation of side products (Figure **S18**).

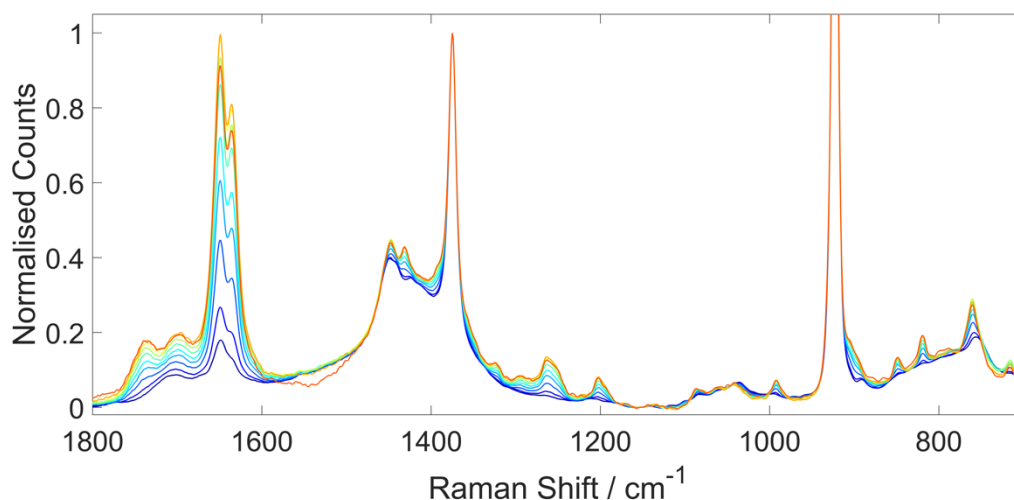


Figure S17 – Normalised Raman spectra of the progression of the thermal reaction with increasing residence time (blue to red) displaying the growth of the characteristic **7a** product modes until 8 min (dark red) where the product yield decreases. This is reflected in a lower intensity of the product's 1650 cm^{-1} vibration.

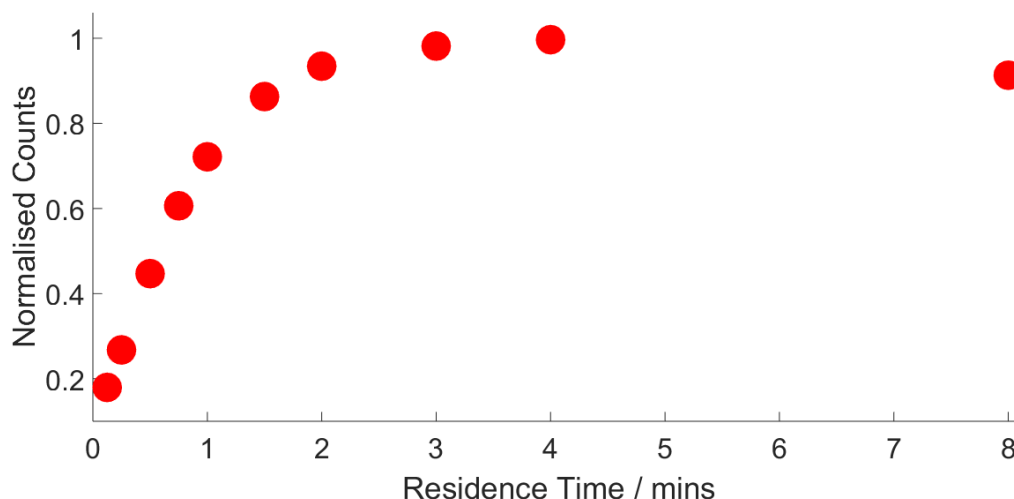


Figure S18 – The intensity of the **7a** product vibration at 1650 cm^{-1} from the normalised Raman spectra of the thermal reaction. This shows the increase in the product yield with increasing residence time until after ca. 5 mins where the yield starts to decrease as side products form.

11. gProms Modelling

Process modelling of the thermal reaction of **5a** to **7a** was carried out using gPROMS modelling software to allow the effect of changing the reaction scale on the performance of the reaction to be investigated, such as would be the case should the Firefly photoreactor be combined with the thermal rig, which would require elevated flow rates.

11.1. Model Description

A schematic of the reactor model is shown in Figure S19, showing a coiled reactor that is placed inside a heating block, depicted in red. The model of the high temperature thermal coil reactor has been developed within Process Systems Enterprise's gPROMS® *ProcessBuilder 1.3.1*. The inner diameter of the reactor tube is 0.305 cm, with a coil diameter of 7 cm and length of 600 cm. The temperature of the heating block, as measured by a K-type thermocouple inside the heating block, is assumed to be the fixed temperature of the reactor wall. The initial concentration concentrations are calculated at standard temperature and pressure, before being introduced into the reactor where it can change depending on conditions.

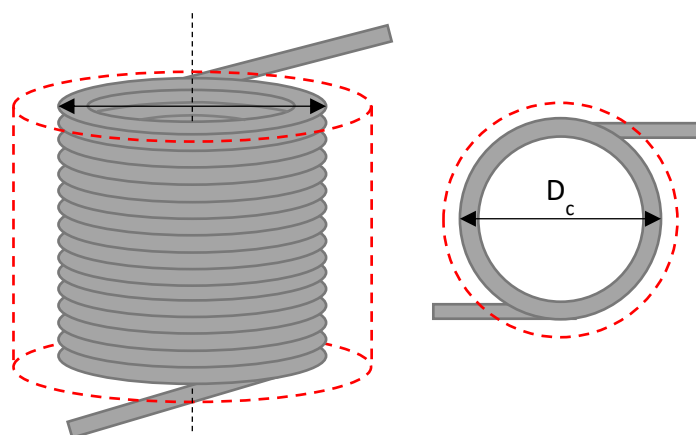
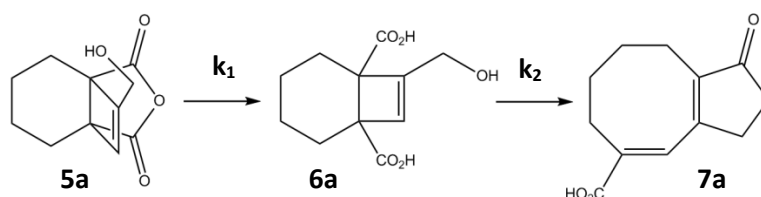


Figure S19 - A schematic of the model, showing the coiled tubular reactor inside a heating block shown in red.

The physical properties, such as density, viscosity or thermal conductivity, of the reaction mixture were calculated using the Peng-Robinson Advanced 1978 (PR-78A) equation of state (EoS).^[8] Due to the low concentration of reagents, the physical properties calculated for this system were assumed to be equal to that of the solvent. The mathematical relationships of the model have been developed from engineering principles so that, with parameter estimation, a semi-empirical model can be developed to predict behaviour outside of the experimental space. The following two reaction scheme (Scheme S7) was initially used, where reaction 1 is hydrolysis of the anhydride motif in **5a** and reaction 2 is the electrocyclic ring opening of **6a**, which occurs via multiple fast-lived intermediates.



Scheme S7 - The two steps of the thermal reaction, where the bridged product (**5a**) of the photochemical step is hydrolysed to **6a**, which then undergoes a rearrangement to form the 8 membered ring compound (**7a**).

12. Density Functional Theory Calculations

Density functional theory (DFT) calculations were carried out for **1a**, $^1[\mathbf{1a}]$, and $^3[\mathbf{1a}]$ using the Q-Chem quantum chemistry software package.^[9] Kohn-Sham DFT calculations of the lowest energy electronic states with singlet and triplet multiplicity (**1a** and $^3[\mathbf{1a}]$) were carried out using the B3LYP exchange-correlation functional and the 6-311G(d,p) electronic basis set.^[10,11] Geometry optimizations, harmonic vibrational frequency calculations and molecular orbital calculations were performed both *in vacuo* and including an explicit solvent model consisting of three MeCN molecules initially positioned around the carbonyl groups. The $^1[\mathbf{1a}]$ excited state was calculated using an excited state DFT self-consistent field procedure during both the geometry optimization and harmonic frequency calculations, in which an electron was moved from the highest occupied molecular orbital (HOMO) to the lowest unoccupied molecular orbital (LUMO) and the maximum-overlap-method was used to prevent variational collapse to the ground state.^[12] Time-Dependent DFT (TDDFT) calculations of electronic excitations from the ground state were carried out using the CAM-B3LYP exchange-correlation functional,^[13] both *in vacuo* and in explicit solvent with a state-specific polarizable continuum model (PCM) solvent with a dielectric constant of 37.5 and an optical dielectric constant of 1.81.

TDDFT calculations indicate that the lowest singlet and triplet electronic excitations of **1a** that correspond to the formation of $^1[\mathbf{1a}]$ and $^3[\mathbf{1a}]$, have $n\pi^*$ and $\pi\pi^*$ orbital excitation character, respectively, when solvated by MeCN (see Table S8 and S9). Orbital analysis in **Figure S20** then shows that the n-orbital involving the carbonyl oxygen atoms becomes increasingly localized onto only one of the two carbonyl groups as the $^1[\mathbf{1a}]$ geometry relaxes. This in turn leads to a change in the bonding of the excited state where the double bonding character in only one of the carbonyl bonds is depleted. This observation is consistent with the presence of the experimental peak at 1762 cm^{-1} in the carbonyl stretching region of the TRIR of **1a**, and a corresponding single carbonyl stretching mode is predicted from the harmonic vibrational analysis of the $n\pi^*$ $^1[\mathbf{1a}]$ species with a vibrational frequency of 1759 cm^{-1} .

Table S8: Dominant orbital contributions and excitation energies (in eV) for the lowest two singlet and triplet electronic excitations of **1a** calculated *in vacuo* using TDDFT.

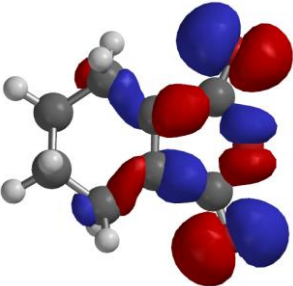
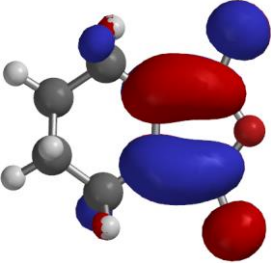
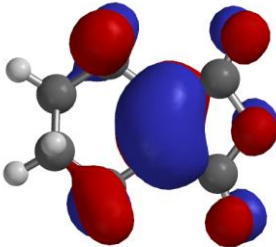
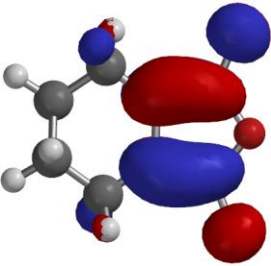
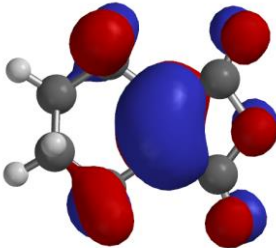
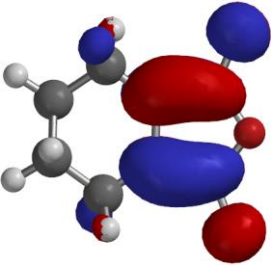
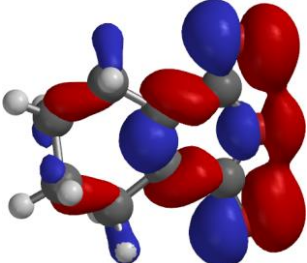
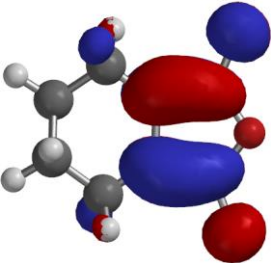
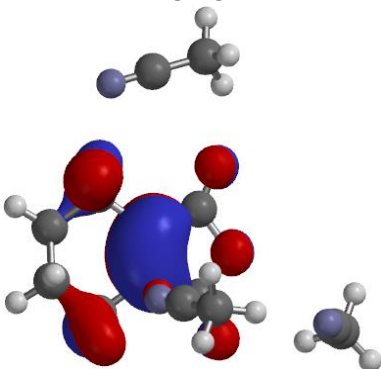
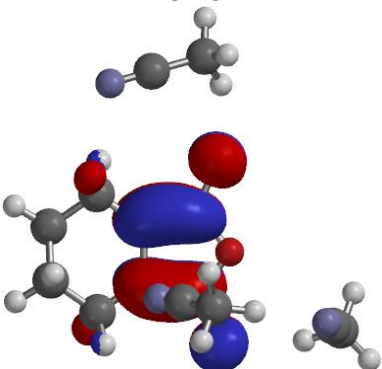
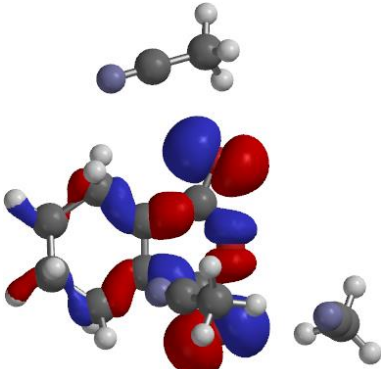
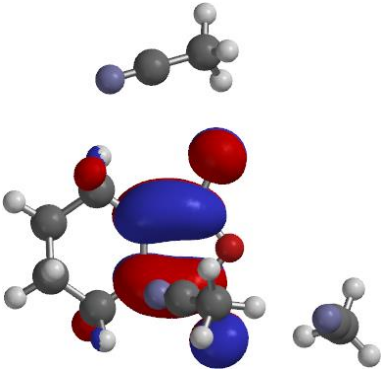
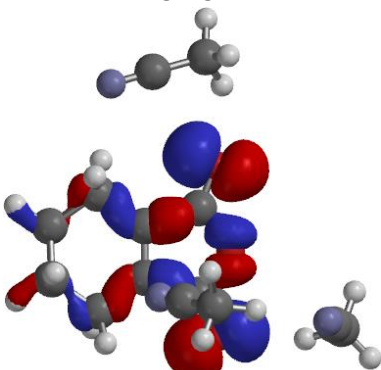
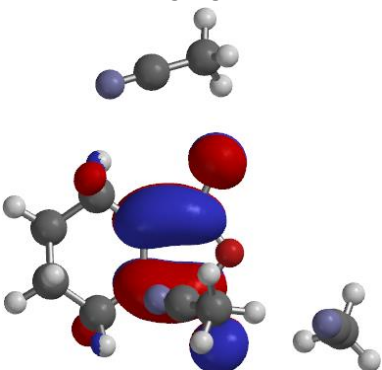
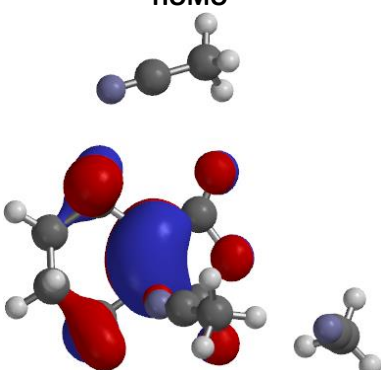
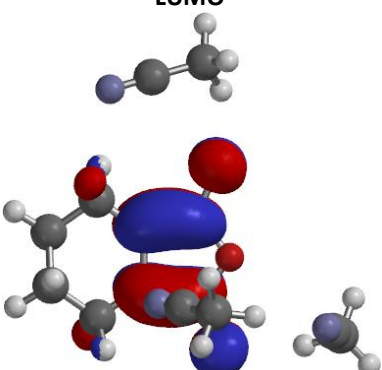
State	Donor MO	Acceptor MO	Excitation Energies
T ₁	HOMO 	LUMO 	3.35
T ₂	HOMO-1 	LUMO 	3.80
S ₁	HOMO-1 	LUMO 	4.25
S ₂	HOMO-2 	LUMO 	4.88

Table S9: Dominant orbital contributions and excitation energies (in eV) for the lowest two singlet and triplet electronic excitations of **1a** calculated in explicit solvent using SS-TDDFT.

State	Donor MO	Acceptor MO	Excitation Energies
T ₁	<p>HOMO</p> 	<p>LUMO</p> 	3.09
T ₂	<p>HOMO-1</p> 	<p>LUMO</p> 	3.98
S ₁	<p>HOMO-1</p> 	<p>LUMO</p> 	4.46
S ₂	<p>HOMO</p> 	<p>LUMO</p> 	4.81

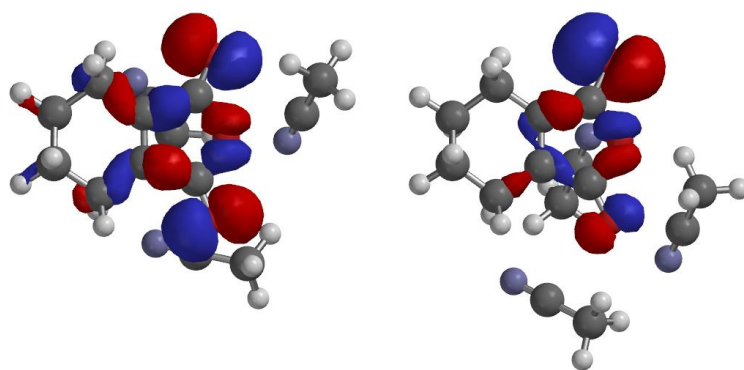


Figure S20 - The highest energy occupied oxygen n-orbital in the ground state electronic configuration shown for the solvated **1a** geometry (left) and **¹[1a]** geometry (right).

13. References

1. Elliott, L. D.; Berry, M.; Harji, B.; Klauber, D.; Leonard, J.; Booker-Milburn, K. I. *Org. Process Res. Dev.* **2016** *20*, 1806-1811.
2. Dudd, L. M.; Venardou, E.; Garcia-Verdugo, E.; Licence, P.; Blake, A. J.; Wilson, C.; Poliakoff, M. *Green Chem.*, **2003**, *5*, 187-192.
3. Hook, B. D. A.; Dohle, W.; Hirst, P. R.; Pickworth, M.; Berry, M. B.; Booker-Milburn, K. I. *J. Org. Chem.*, **2005**, *70*, 7558-7564.
4. Booker-Milburn, K. I.; Cowell J. K.; Delgado-Jiménez, F.; Sharpe, A.; White A. J. *Tetrahedron*, **1999**, *55*, 5875-5888.
5. Ralph, M. J.; Harrowven, D. C.; Gaulier, S.; Ng, S.; Booker-Milburn, K. I. *Angew. Chemie - Int. Ed.* **2015**, *54*, 1527-1531.
6. a) Booker-Milburn, K. I.; Delgado-Jimenez, F.; Sharpe, A. *Tetrahedron*, **1999**, *55*, 5889-5902. b) Booker-Milburn, K. I.; Cowell, J. K.; Harris, L. J. *Tetrahedron*, **1997**, *53*, 12319-12338.
7. Brennan, P.; George, M. W.; Jina, O. S.; Long, C.; McKenna, j.; Pryce, M. T.; Sun, X.; Vuong, K. Q. *Organometallics*, **2008**, *27*, 3671-3680.
8. Robinson D. B.; Peng, D. Y. The characterization of the heptanes and heavier fractions for the GPA Peng–Robinson programs, Gas processors association. (**1978**).
9. Shao, Y.; Gan, Z.; Epifanovsky, E.; Gilbert, A.T.B.; Wormit, M.; Kussmann, J.; Lange, A.W.; Behn, A.; Deng, J.; Feng, X.; Ghosh, D.; Goldey, M.; Horn, P.R.; Jacobson, L.D.; Kaliman, I.; Khaliullin, R.Z.; Kuś, T.; Landau, A.; Liu, J.; Proynov, E.I.; Rhee, Y.M.; Richard, R.M.; Rohrdanz, M.A.; Steele, R.P.; Sundstrom, E.J.; Woodcock, H.L.; Zimmerman, P.M.; Zuev, D.; Albrecht, B.; Alguire, E.; Austin, B.; Beran, G.J.O.; Bernard, Y.A.; Berquist, E.; Brandhorst, K.; Bravaya, K.B.; Brown, S.T.; Casanova, D.; Chang, C.-M.; Chen, Y.; Chien, S.H.; Closser, K.D.; Crittenden, D.L.; Diedenhofen, M.; DiStasio, R.A.; Do, H.; Dutoi, A.D.; Edgar, R.G.; Fatehi, S.; Fusti-Molnar, L.; Ghysels, A.; Golubeva-Zadorozhnaya, A.; Gomes, J.; Hanson-Heine, M.W.D.; Harbach, P.H.P.; Hauser, A.W.; Hohenstein, E.G.; Holden, Z.C.; Jagau, T.; Ji, C.H.; Kaduk, B.; Khistyayev, K.; Kim, J.; Kim, J.; King, R.A.; Klunzinger, P.; Kosenkov, D.; Kowalczyk, T.; Krauter, C.M.; Lao, K.U.; Laurent, A.D.; Lawler, K.V.; Levchenko, S.V.; Lin, C.Y.; Liu, F.; Livshits, E.; Lochan, R.C.; Luenser, A.; Manohar, P.; Manzer, S.F.; Mao, S.-P.; Mardirossian, N.; Marenich, A.V.; Maurer, S.A.; Mayhall, N.J.; Neuscamman, E.; Oana, C.M.; Olivares-Amaya, R.; O'Neill, D.P.; Parkhill, J.A.; Perrine, T.M.; Peverati, R.; Prociuk, A.; Rehn, D.R.; Rosta, E.; Russ, N.J.; Sharada, S.M.; Sharma, S.; Small, D.W.; Sodt, A.; Stein, T.; Stück, D.; Su, Y.-C.; Thom, A.J.W.; Tsuchimochi, T.; Vanovschi, V.; Vogt, L.; Vydrov, O.; Wang, T.; Watson, M.A.; Wenzel, J.; White, A.; Williams, C.F.; Yang, J.; Yeganeh, S.; Yost, S.R.; You, Z.-Q.; Zhang, I.Y.; Zhang, X.; Zhao, Y.; Brooks, B.R.; Chan, G.K.L.; Chipman, D.M.; Cramer, C.J.; Goddard, W.A.; Gordon, M.S.; Hehre, W.J.; Klamt, A.; Schaefer, H.F.; Schmidt, M.W.; Sherrill, C.D.; Truhlar, D.G.; Warshel, A.; Xu, X.; Aspuru-Guzik, A.; Baer, R.; Bell, A.T.; Besley, N.A.; Chai, J.-D.; Dreuw, A.; Dunietz, B.D.; Furlani, T.R.; Gwaltney, S.R.; Hsu, C.-P.; Jung, Y.; Kong, J.; Lambrecht, D.S.; Liang, W.; Ochsenfeld, C.; Rassolov, V.A.; Slipchenko, L.V.; Subotnik, J.E.; Van Voorhis, T.; Herbert, J.M.; Krylov, A.I.; Gill, P.M.W.; Head-Gordon, M. *Mol. Phys.*, **2014**, *113*, 184-215.
10. Becke, A. D. *J. Chem.*, **1993**, *98*, 5648-5652.

11. Stephens, P. J.; Devlin, F. J.; Chabalowski, C. F.; Frisch, M. J. *J. Phys. Chem.*, **1994**, *98*, 11623-11627.
12. Gilbert, A. T. B.; Besley, N. A.; Gill, P. M. W. *Phys. Chem. A*, **2008**, *112*, 13164-13171.
13. Yanai, T.; Tew, D. P.; Handy, N. C. *Chem. Phys. Lett.*, **2004**, *393*, 51-57.